UNIVERSITY OF CRETE
DEPARTMENT OF PHYSICS
&
FOUNDATION FOR RESEARCH AND TECHNOLOGY
HELLAS - INSTITUTE OF ELECTRONIC STRUCTURE AND LASER

IESL - FORTH

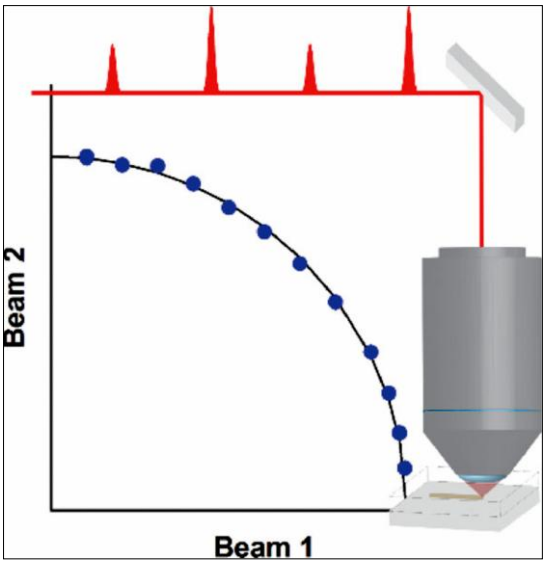

In situ measurement of the effective nonlinear absorption order in multiphoton photoresists[1]

Master Thesis of Dimitra Ladika

Supervisor
Maria Farsari

Co-Supervisors
Ioanna Sakellari
&
David Gray

HERAKLION, SEPTEMBER 2018

Contents

Ευχαριστίες

Για την εκπόνηση της παρούσας μεταπτυχιακής εργασίας θα ήθελα να ευχαρηστήσω αρχικά την κ. Φαρσάρη η οποία μου έδωσε την ευκαιρία να δουλέψω στο εργαστήριο της καθώς και για την εμπιστοσύνη που μου έδειξε για να στήσω την συγκεκριμένη πειραματική διάταξη.
Στη συνέχεια, καθοριστικό ρόλο στην πραγματοποίηση της πειραματικής διάταξης είχαν η Μεταδιδάκτορας Ιωάννα Σακελλάρη και Dr. David Gray οι οποίοι με τις γνώσεις τους, την εμπειρία τους και το ενδιαφέρον τους συνέβαλλαν στο να κατανοήσω εις βάθος το θεωρητικό υπόβαθρο της τεχνικής αυτής καθώς και να καταφέρω να στήσω το πείραμα αυτό.
Θα ήθελα επίσης να ευχαριστήσω την κ.Λουκάκο και τον κ.Χαραλαμπίδη που μου έκαναν την τιμή να είναι στην τριμελή επιτροπή μου.
Επίσης, ευχαριστώ θερμά όλα τα παιδιά από το group της Μη-Γραμμικής Λιθογραφίας και συγκεκριμένα την Ελμίνα Καμπουράκη, την Dr.Βασιλεία Μελισσινάκη, τον Γιάννη Σπανό, την Μαρία Μανουσιδάκη και ιδιαίτερα τον Κώστα Παρκάτζε, οπού με ενθάρρυνε και με βοήθησε τις φορές που δυσκολεύτηκα κατά την διάρκεια της εκπόνησης της μεταπτυχιακής μου εργασίας, δημιουργώντας ευχάριστο κλίμα.
Ευχαριστώ επίσης τον Μιχάλη Λουλάκη και τον Γιάννη Λαμπράκη για την τεχνική τους υποστήριξη καθώς και την κα. Αλέκα Μανουσάκη, για την συνεργασία της στο ηλεκτρονικό μικροσκόπιο σάρωσης, SEM.
Τέλος, ευχαριστώ την οικογένεια μου και ιδιαίτερα την αδερφή μου Αναστασία, όπως και τους φίλους μου.

Abstract

The basis of direct laser writing by multi-photon polymerization (MPP) is the phenomenon of multi-photon absorption (MPA). Knowledge of the order of the effective nonlinear absorption in multiphoton photoresists is a key element in the development of improved materials for multiphoton absorption polymerization (MAP). However, due to the low probability of the MPA processes, their accurate characterization remains a challenge. In this work, a new technique is introduced, named Two-Beam Initiation Threshold (2-BIT), in order to determine the order of the effective nonlinear absorption in a series of photoinitiators using a simple optical arrangement that can be employed with almost any MPP setup. The photoinitiators characterized were both commercial and lab-synthesized. The linear absorption spectrum is demonstrated to be a poor predictor of the effective order of nonlinear absorption at a given wavelength. Also, 3D structures were fabricated using MPP, in order to determine the resolution of these photoinitiators.

ΠΕΡΙΛΗΨΗ

Ο πολυφωνικός πολυμερισμός είναι μια τεχνική απευθείας γραφής με λέιζερ η οποία έχει σκοπό την κατασκευή τρισδιάστατων νανοδομών, με ανάλυση μερικών δεκάδων νανομέτρων. Το φαινόμενο στο οποίο βασίζεται ο πολυφωτονικός πολυμερισμός είναι η μη γραμμική απορρόφηση ή πολυφωτονική απορρόφηση, διαδικασία κατά την οποία δύο ή περισσότερα φωτόνια απορροφώνται από φωτοευαίσθητα μόρια και διεγείρονται. Τα φωτοευαίσθητα αυτά μόρια ονομάζονται φωτοεκκινητές και χρησιμοποιούν το φαινόμενο της μη γραμμικής απορρόφησης για την παραγωγή ριζών οι οποίες συμβάλλουν στην εκκίνηση του πολυμερισμού. Ο μηχανισμός που πραγματοποιείται συνήθως για τον πολυφωτονικό ποολυμερισμό είναι ο μηχανισμός ελευθέρων ριζών.

Οι φωτοεκκινητές και πιο συγκεκριμένα ο μη γραμμικός οπτικός χαρακτηρισμός τους έχει αποτελέσει πρόκληση για την επιστημονική κοινότητα καθώς η γνώση της τάξης της μη γραμμικής απορρόφησης τέτοιων φωτοευαίσθητων μορίων συμβάλλει στην αναβάθμισης της σύνθεσης των υλικών που χρησιμοποιούνται στον πολυφωτονικό πολυμερισμό.

Στην παρούσα μεταπτυχιακή εργασία θα παρουσιάσουμε μια νέα τεχνική, που ονομάζεται Two-Beam Initiation Threshold (2-BIT) και σκοπό έχει τον προσδιορισμό της τάξης της μη γραμμικής απορρόφησης κάποιων νέων αλλά και ευρέως γνωστών, φωτοεκκινητών. Η τεχνική 2-BIT, αποτελεί μια απλή οπτική διάταξη η οποία μπορεί να αναπτυχθεί σε οποιοδήποτε εργαστήριο που πραγματοποιεί πολυφωτονικό πολυμερισμό.

Chapter 1

1.1 Nonlinear Optics

Nonlinear optics is a phenomenon, can be seen in certain materials when intense light is shown to those materials. It is the modification of natural optical properties by the presence of light. Typically, any intense laser light is enough to produce these phenomena. Nonlinear optical phenomena are “nonlinear" in the sense that, they occur when the response of a material to an applied optical field depends in a nonlinear manner on the strength of the applied field.

For weak optical fields that are applied to a material, the induced polarization is $\vec{P}(t)$ proportional to the electric field $\vec{E}(t)$:

$$\vec{P}(t) = \varepsilon_o \chi_e \vec{E}(t) \qquad (1)$$

where χ_e is the linear susceptibility and ε_o is permittivity in free space. This is the case of linear optics.
In contrast with the linear optics, in nonlinear optics the polarization depends on the electric field as given below:

$$\vec{P} = \chi^{(1)}\vec{E} + \chi^{(2)}\vec{E}^2 + \chi^{(3)}\vec{E}^3 + \cdots = \vec{P}^{(1)} + \vec{P}^{(2)} + \vec{P}^{(3)} + \cdots \qquad (2)$$

Where $\chi^{(i)}$ is the i-th order susceptibility. The susceptibilities are complex numbers, where the real part corresponds to the nonlinear refractive index and the imaginary part to nonlinear absorption coefficient. Actually, the nonlinear susceptibilities are tensors and depend on the frequencies of the applied fields. For example, $\chi^{(3)}$ is, in general, a complex fourth-rank tensor with elements $\chi^{(3)}_{ijkl}(-\omega_3, \omega_1, \omega_1, -\omega_2)$, where the subscripts on the susceptibility denote the polarizations of the three input fields and the output field . Specifically, the imaginary part of $\chi^3(-\omega, \omega, \omega, -\omega)$ is related to the two-photon absorption (2PA)[2], whereas the real part is related to nonlinear refraction. Concerning the second allowed nonlinear term for materials with inversion symmetry is the fifth-order nonlinear susceptibility $\chi^{(5)}$ and with the similar manner , the real part of $\chi^{(5)}$ for a single input frequency and the same signal frequency is related to a refractive index change that depends on the intensity squared, whereas the imaginary part can be related to three-photon absorption (3PA).

1.2 Nonlinearities due to Two-Photon Absorption

Two-photon absorption was first theoretically described by Maria Goeppert-Meyer[3] in 1932, but first observed by Kaiser and Garrett in 1961 right after the invention of the laser. In 2PA, two quanta of light are simultaneously absorbed to promote an atom, ion, or solid from a lower energy state to a higher energy state as illustrated in **Figure 1.**

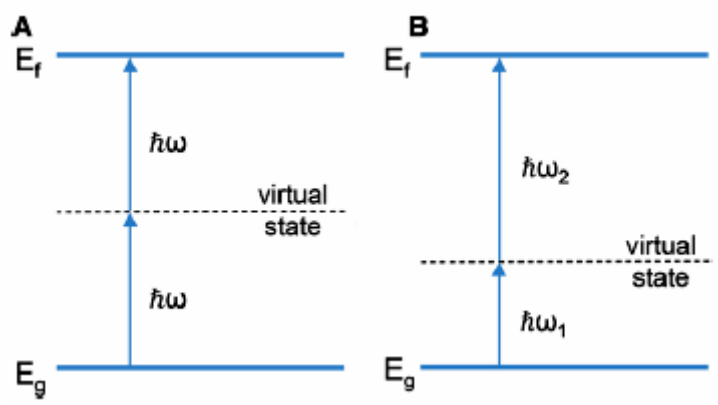

Fig. 1

Figure 1A illustrates degenerate 2PA, in which two photons of frequency ω drive a resonant transition at frequency 2ω. **Figure 1B** illustrates nondegenerate 2PA, in which photons of two different frequencies, ω_1 and ω_2, drive a resonant transition at frequency $\omega_1 + \omega_2$.

The two-photon absorption (2PA) coefficient $\boldsymbol{\alpha}^{(2)}$ is an important characteristic of optical materials, in particular, for the nonlinear ones which are often employed at high intensities. Therefore, the derivation of the 2PA coefficient will be presented below.

In media with inversion symmetry, almost all of the 81 tensor components of $\chi^{(3)}$ vanish and only four of them are unique: $\chi^{(3)}_{xxxx}(-\omega_3, \omega_1, \omega_1, -\omega_2)$, $\chi^{(3)}_{xxyy}(-\omega_3, \omega_1, \omega_1, -\omega_2)$, $\chi^{(3)}_{xyxy}(-\omega_3, \omega_1, \omega_1, -\omega_2)$, $\chi^{(3)}_{xyyx}(-\omega_3, \omega_1, \omega_1, -\omega_2)$.[2]The relation between these elements is:

$$\chi^{(3)}_{xxxx} = \chi^{(3)}_{xxyy} + \chi^{(3)}_{xyxy} + \chi^{(3)}_{xyyx} \qquad (3)$$

In case of a nonlinear refractive index, applies: $\chi^{(3)}_{xxyy}(-\omega, \omega, \omega, -\omega) = \chi^{(3)}_{xyxy}(-\omega, \omega, \omega, -\omega)$, so that only two elements are independent.

$$\chi^{(3)}_{xxxx} = 2\chi^{(3)}_{xxyy} + \chi^{(3)}_{xyyx} \qquad (4)$$

For a single, linearly polarized laser beam the quadratic nonlinear refractive index η_2 is related to the third-order susceptibility by

$$n_2\,(esu) = \frac{12\pi}{n_0}\ \ \chi^{(3)}_{xxxx}\,(esu) \qquad (5)$$

where *esu* denotes the electrostatic units (cm^3/erg) and n_o is the linear refractive index of the medium. For Kerr nonlinearity the refractive index of the material is given by

$$n = n_o + n_2\frac{|\bar{E}|^2}{2} = n_o + \gamma' I \qquad (6)$$

where E is the complex electric field, I is the irradiance and γ' is the nonlinear refractive parameter, which is related to the quadratic nonlinear refractive index through

$$n_2\,(esu) = \frac{cn_o}{40\pi\gamma'}\,(m^2/w) \qquad (7)$$

The 2PA coefficient $\boldsymbol{\alpha}^{(2)}$ is directly proportional to the imaginary part of the third-order susceptibility through[4]

$$\alpha^{(2)}\,(esu) = \frac{96\pi^2\omega}{n_o^2\,c^2}\,Im\chi^3(esu) \qquad (8)$$

where $\boldsymbol{\alpha}^{(2)}$ is given in *esu*, η_o is the linear refractive index of the medium, *c* is the speed of light in cm s^{-1}, and ω is the fundamental frequency in radians s^{-1}. The conversion formula between the CGS and SI systems of units is given by[2]

$$\chi^{(3)}(SI) = \frac{4\pi}{3^2} \times 10^{-8}\,\chi^{(3)}\,(esu) \qquad (9)$$

On an atomic (or molecular) level, the electric field in Eq. (2) is replaced by the local electric field E_{loc}, which for isotropic media is related to the incident electric field through the relation:

$$E_{loc} = LE \qquad (10)$$

where $L = \frac{(n_0^2+2)}{3}$ is the Lorentz- Lorenz local field correction factor.

Therefore, for third-order nonlinear effects, the corresponding hyperpolirizability γ is related to the third-order susceptibility $\chi^{(3)}$ by

$$\gamma = \chi^{(3)}/NL^4 \qquad (11)$$

In order to be accurate should be mentioned that hyperpolirizabilities describe the induced nonlinear polarization per molecule. So, N is the number of the molecules per unit volume. The hyperpolirizability γ is independent of concentration.[5]

1.2 Brief Formulations of MPA-Induced Light Attenuation

At sufficiently high irradiances, the nonlinear response of a medium gives rise to multiphoton absorption (MPA). MPA is the simultaneous absorption of two or more photons, where the combined energy of the absorbed photons exceeds the energy bandgap of the medium. The number of photons that are simultaneously absorbed depends on the photon energy and the energy bandgap of the medium and is sometimes referred to as the multiphoton order. Since MPA is a nonlinear interaction, it only occurs in a highly localized volume, at the focus of a laser beam for example, and can occur deep within the bulk of a transparent material**.** [6]

The attenuation of a light beam passing through an optical medium can be generally expressed by the following phenomenological expression[7]:

$$\frac{dI(z)}{dz} = -\alpha^{(1)}I(z) - \alpha^{(2)}I^2(z) - \alpha^{(3)}I^3(z) - \alpha^{(4)}I^4(z) \ldots. \qquad (12)$$

Here I (z) is the intensity of the incident light beam propagating along the z-axis and a, β, γ and η are the one-, two-, three-, and four-photon absorption coefficients of the transmitting medium, respectively. When 2PA is the only nonlinear absorption process driven by single-beam excitation, we have:

$$\frac{dI(z,t)}{dz} = -\alpha^{(1)}I(z,t) - \alpha^{(2)}I^2(z,t) \qquad (13)$$

The physical meaning of this expression is that the 2PA probability of molecules in a given position is proportional to the square of the local light intensity. The solution of eq. (13) which is for the irradiance at the back surface of the medium of thickness l yields:

$$I(l, t + \Delta t) = \frac{(1-R)^2\, I(0,t)\exp(-\alpha^{(1)}l)}{1+\alpha^{(2)}(1-R)I_0 l_{eff}} \qquad (14)$$

where R is the surface reflectance, I (0,t) is the incident instantaneous irradiance, Δt is the amount of time it takes for light to traverse the sample and $\boldsymbol{l_{eff} = \frac{1-exp(-al)}{a}}$ is the effective sample length.

The 2PA coefficient $\alpha^{(2)}$ is a macroscopic parameter that depends on molecular concentration. To compare experimental absorption nonlinearities between different molecules, it is common practice to describe two-photon nonlinearity by means of the molecular 2PA cross section σ_2 , which is a molecular constant that is independent of the concentration. The relation between $\alpha^{(2)}$ (in cm/GW) and σ_2 (in cm^4/GW) is:

$$\alpha^{(2)} = \sigma_2 N_0 = \sigma_2 N_A C \times 10^{-3} \qquad (15)$$

where N_0 is the molecular density of the compound (in cm^{-3}) and N_A is Avogadro's number and C the molar concentration.

Another expression for the 2PA cross section is: $\sigma_2 = \frac{\hbar\omega\alpha^{(2)}}{N}$ (16)

In which $\hbar\omega$ is the photon energy. The units for the 2PA cross section are cm^4 or Goppert-Mayer (GM)[6], which is equal to 10^{-50} cm^4s.

At this point, we have to generalize in the case of an n-photon absorption process. The eq. (13) can now be recast as:

$$\frac{dI(z,t)}{dz} = -\alpha^{(1)}I(z,t) - \alpha^{(n)}I^n(z,t) \quad (17)$$

The units of the n-th order absorption coefficient $\alpha^{(n)}$ are cm^{2n-3}/GW^{n-1} and the n-photon absorption cross section is given by:

$$\sigma_n = \frac{\hbar\omega\alpha^{n-1}}{N} \quad (18)$$

The solution for the instantaneous irradiance at the far surface of a medium of thickness l is then:

$$I(l, t+\Delta t) = \frac{(1-R)^2\, I(0,t)\exp(-\alpha^{(1)}l)}{\left[1+n\alpha^{n+1}\left[\frac{1-\exp(-n\alpha^{(1)}l)}{n\alpha^{(1)}}\right](1-R)^n I^n(0,t)\right]^{1/n}} \quad (19)$$

At this point we have to determine the terms that will be used in this thesis in order to indicate the magnitude squared of a light field. The radiant flux incident on a unit area of a material is called irradiance and in SI units is given in W/m^2. The instantaneous irradiance I (z, t) of a complex electric field[7]:

$$\mathbf{E} = \frac{1}{2}\mathbf{E}_0 e^{i(\omega t-kz)} + \frac{1}{2}\mathbf{E}_0^* e^{-i(\omega t-kz)} \quad (20)$$

travelling in the vacuum is given by:

$$I(z, t) = c\varepsilon_0|E|^2 = c\varepsilon_0 E_0^2\cos^2(\omega t - kz) \quad (21)$$

Because typical detectors cannot respond to oscillations of light waves at $\omega \sim 10^{13} - 10^{15}$ Hz in the visible and near-infrared region regions of the spectrum, they instead measure the time-averaged irradiance

$$\langle I\rangle = \frac{c\varepsilon_0|E|^2}{T}\int_0^T \cos^2(\omega t - kz)dt = \frac{1}{2}c\varepsilon_0|E|^2 \text{ (SI)} \qquad (22)$$

or

$$\langle I\rangle = \frac{c}{8\pi}|E|^2 \text{ (cgs)} \qquad (23)$$

The strength of a linear optical process is proportional to the time-averaged irradiance. For nonlinear processes, it is typically the peak irradiance *Imax* that is important, along with the pulse shape and the repetition rate of the laser. For a laser with temporal and spatial profiles that are Gaussian, the peak on-axis irradiance is

$$I_{max} = 4\frac{\sqrt{\ln 2}E}{\pi^{3/2}\omega_0^2\ \tau} \qquad (24)$$

where E is the pulse energy measured with an energy meter, w_0 is the beam waist at the focal plane, and τ is the pulse duration (full width at half maximum). The pulse shape affects the relative efficiency of absorptive processes of different orders, so for simplicity we will assume "square" pulses in the following unless otherwise noted. Note also that so long as the pulse length is held constant, $\langle I\rangle$ and I_{max} scale with one another and so the former quantity is often the one reported. However, detailed knowledge of the laser pulse shape is required for the accurate determination of MPA cross sections, especially when multiple nonlinearities are present simultaneously.

1.4 Abbe's Diffraction Limit

Every optical imaging system can be limited by experimental factors, such as errors in alignments or imperfections in its optical components. But there is a fundamental limit for the maximum resolution every optical imaging system can achieve. That limit is called Abbe's diffraction limit[8] and is an effect of the diffraction of light [90]. Focused light travelling through a medium creates a spot with radius,

$$d = \frac{\lambda}{2*n*sin\theta} \qquad (25)$$

Where λ: wavelength of light (nm), n: diffraction coefficient of medium and θ: angle of convergence.

The product n*sinθ is called numerical aperture (NA). In modern optics NA ranges from 1.4~1.6. So, for the spectrum of visible wavelengths (400nm-700nm), the focusing spot ranges from 0.14μm~0.25μm. The wavelength can be reduced to achieve higher resolution, but smaller wavelength means higher energy/photon, so the risk of damaging the sample is increased.

1.5 Cross-section in the focused spot for single and multi-photon absorption

When a laser beam is closely focused with a high NA objective lens into a volume of photo-curable resin, as shown in **Figure 2a**, photon-density-profiles are formed, with a constant total number of photons at every cross-section in the focused spot.

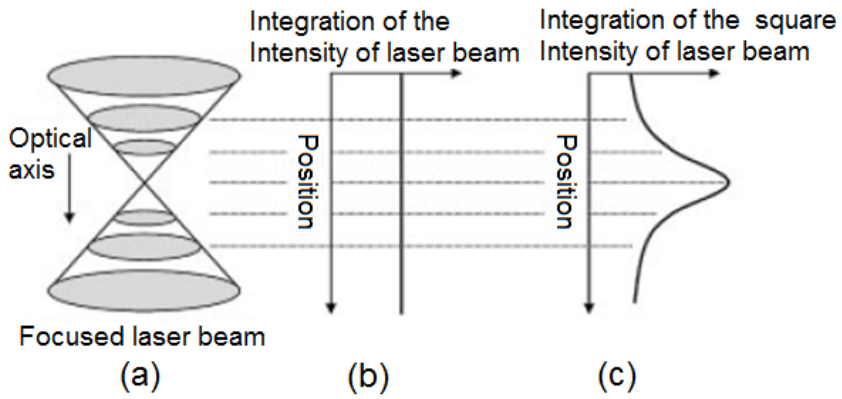

Fig 2. *Comparison of TPA with single photon absorption generated by a tightly focused laser beam: (a) schematic diagram of focused laser beam, (b) total single photon absorption per transverse plane, (c) total two photon absorption per transverse plane, which is calculated by integrating the square intensity over the plane with respect to the optical axis.* ***(Taken from*** **[9])**

The constant number of photons at every cross-section precludes optical sectioning by exploiting the linear response of materials to the light intensity based on the single photon absorption (see **Figure.2b**). However, if the material response is proportional to the square of the photon density, the integrated material response is greatly enhanced at the focal point, as illustrated in **Figure 2c**. The two photon transition rate is extremely small in general, so a very high spatial resolution can be obtained.

1.6 Description of polymerization based on radical initiators

Photopolymerization is one of the most important types of photochemical reaction that have been used for laser fabrication. This is because the material resins undergo a significant phase transition after laser irradiation, from liquid/gel to solid, and non-polymerized liquid is easily removed by a developing process so that the solidified 3D structures stand out. The basic components of the starting liquid material are monomers. Upon light excitation, the monomers may be solidified by polymerization [10].

Photo-polymerization is realized via chain reactions as shown in Equation 25, so the quantum yield can reach several thousands.

$$M \xrightarrow{M} M_2 \xrightarrow{M} M_3 ... M_{n-1} \xrightarrow{M} M_n \qquad (25)$$

Here M is the monomer or oligomer unit, and M_n, the macromolecule containing n monomer units. The quantum yield of general monomers is low. In order to increase the initiating efficiency, one or several low-weight molecules that are more sensitive to light irradiation are added. They form initiating species of radicals or cautions by absorbing photons. Such small molecules are called photo-initiators:

$$I \xrightarrow{\frac{\square\nu}{2}, \frac{\square\nu}{2}} I^* \rightarrow R\cdot \qquad (26)$$

where I denote the photo-initiator, R· the free radicals and I^* an intermediate state of the photo-initiator after absorbing the photons. Therefore the polymerization process is more precisely described by the following equation:

$$R\cdot + M \rightarrow RM\cdot \xrightarrow{M} RMM\cdots \rightarrow RM_n\cdot \qquad (27)$$

The photo-produced radicals react with monomers, producing monomer radicals, which combine with new monomers, and so on; so the monomer radicals expand in chain reaction, until two radicals meet with each other. This chain propagation stops in either of the following channels:

$$RM_n\cdot + RM_m\cdot \rightarrow RM_{m+n}R \qquad (28)$$

$$RM_n\cdot + RM_m\cdot \rightarrow RM_n + RM_m \qquad (29)$$

Therefore the polymerization process consists of three steps: (I) photo-initiation, (ii) chain propagation, and (iii) termination[11].

A good photo-initiator should be easily reduced to an initiating species upon light irradiation, and provide photo-produced radicals or cautions active enough to react with monomers.

The nonlinear response of photo-polymerization is caused by highly reactive oxygen molecules absorbed by resin. Oxygen molecules inhibit polymerization reaction at the beginning of polymerization, because oxygen molecules scavenge the radicals that generate the polymerization reaction. Accordingly, when the intensity of light is adequately low polymerization reaction does not propagate, because almost all the photons are consumed by the oxygen molecules.

A photo-sensitizer is a molecule that absorbs light and then transfers the energy to a photo-initiator. With such a scheme, the photo-initiation process is expressed as

$$S \xrightarrow{\frac{h\nu}{2}\cdot\frac{h\nu}{2}} S^* \ldots \xrightarrow{I} I^* \rightarrow R\cdot \qquad (30)$$

where S is the photo-sensitizer. A co-initiator itself does not absorb light, but it is involved in the production of radical species. Reactions that are typically used for laser fabrication are double-bond addition of acrylates (radical-type)

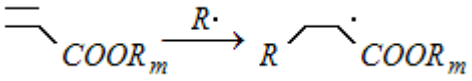

(31)

For a radical type initiator, benzoyl is the most widely used chromophore, which must have the initiator, since it exhibits good absorption in the UV region.

After polymerization, the oligomer constitutes the backbone of the polymer network. The physical, chemical and mechanical properties of the solidified resin in strictly depend on the nature and structure of the oligomer. Oligomers generally contain at least two reactive groups, from which both cross-linking and polymerization could occur.

Monomers have a much smaller molecular weight and consist of one or several reactive groups. They polymerize similarly to oligomers and are an important factor in determining the efficiency of polymerization. In addition, monomers are also useful for diluting resins so that the polymer is easier to handle for a particular use.[12]

For 3D micro-nanolithography, a suitable viscosity is of particular importance due to the opposite requirements in different steps of processing: a high viscosity is needed for keeping early produced volumes where they are created; while a low viscosity facilitates removal of unsolidified resin from intervals. For a successful fabrication the following behaviors are preferred: i) high polymerization efficiency upon light irradiation, (ii) lower shrinkage after polymerization, (iii) fast reaction time and low dark polymerization.

1.6 MPA and processes occurring in the excited-states

The discussion will now be focused on the processes occurring in the excited states in case of 2PA.

The diagram below (Fig.3) describes those processes. Due to a long excited-state lifetime, the triplet state (where the sum of the electronic spin in a molecule is 2s+1=3, where s= 1/2 or -1/2 is the quantum number of the electronic spin) is the major transient state that is responsible for the generation of radicals.

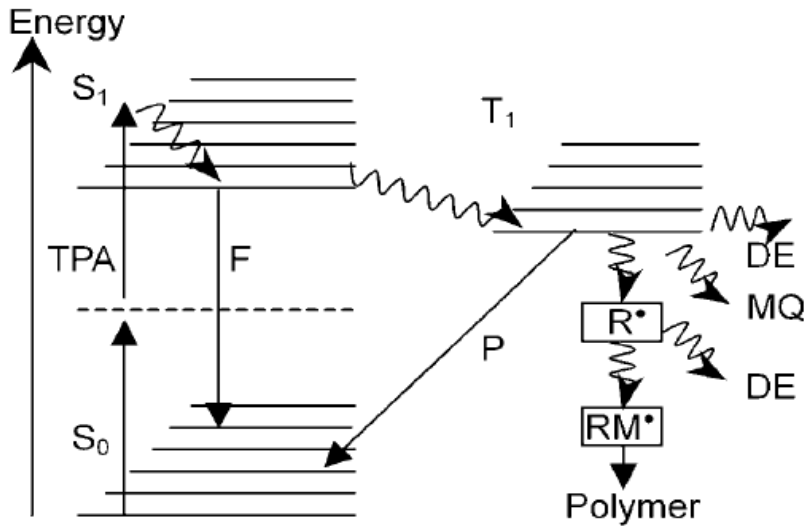

Figure 3 *Processes occurring in the excited-states[Taken from* [11]*]*

The steps that take place in this diagram are:

- Valence electrons of an initiator are excited from the ground (S_0) to the first excited (S_1) singlet state by simultaneously absorbing two photons.

- The excited electrons then relax by transition to the triplet state (T_1) via intersystem crossing, where the initiator is liable to undergo bond cleavages, producing radicals for photopolymerization.

- The excited states can also be relaxed by radiative processes: fluorescence emission from singlet states (F) or phosphorescence emission from triplet states (P).

- Both the triplet state and photoproduced radicals can be deactivated (DE), for example by monomer quenching (MQ) for the former, and by radical quenching (RQ) for the latter.

Efficient photopolymerization generally needs these competing processes (F, P, DE) minimized but there are a few cases, for instance RQ, which find use for it in reducing voxel sizes. The dashed line denotes a virtual energy level for TPA.

1.7 Excited-state Absorption (ESA)

The above discussion considers instantaneous polarization effects involving strictly ultrafast nonlinearities (in the fs regime) through virtual or bound intermediate excited states. However, some nonlinear optical processes involve population redistribution among real states. The efficiency of such processes depends on the pulse width of the

laser excitation.[13] The most common such transient mechanism is ESA. In a molecular system that is n-photon resonant at the excitation wavelength, at sufficiently high irradiance the excited state can be populated significantly. If this excited state can also absorb light at the excitation wavelength, ESA can contribute to the total absorption cross section. ESA transitions must occur before molecules in the first excited state decay back to the ground state.

To give insight into the ESA process, Fig. 4 shows a three level energy diagram. The absorption of an incident photon initially promotes a molecule to the manifold of vibrational levels of the first electronic excited singlet state, S_1. From there the molecule will undergo rapid relaxation (on a ps timescale) to the lowest vibrational level of S_1[14]. The molecule can then either absorb another photon to be promoted to the second excited singlet state, S_2, or relax back to the ground state radiatively or nonradiatively. The associated transition rate constant for this latter process is k_{10}. If the molecule is promoted to S_2, it can either relax back to S_1 with a transition rate constant k_{21} or directly to the ground state S_0 with a rate constant k_{20}.

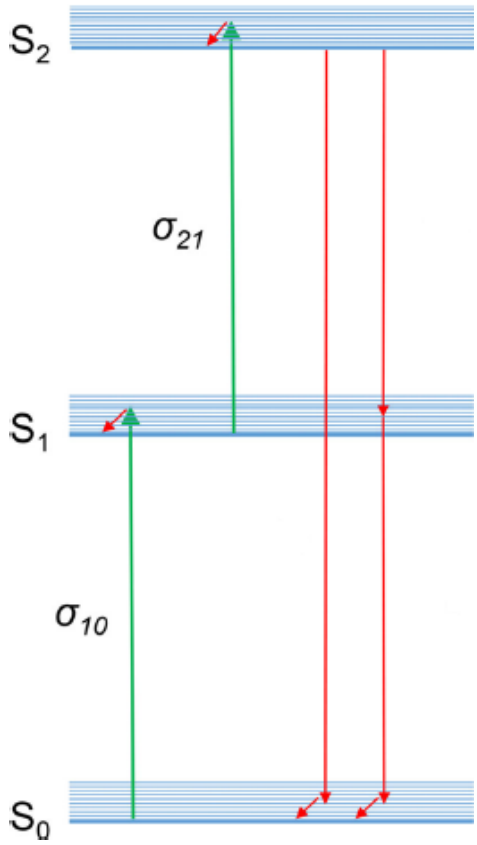

Fig. 4

Generally, when the irradiance/fluence is increased, ground-state depletion becomes important. For these reasons, it is common to use an effective nonlinear absorption coefficient,$\alpha_{eff}^{(2)}$, to describe two step ESA that involves population redistribution. Furthermore, $\alpha_{eff}^{(2)}$ can also depend on the pulse duration, in the case of the pulse duration being longer than the decay times. Furthermore, for pulse widths long

enough to be comparable to the intersystem crossing time, triplet states should be also expected to contribute significantly to ESA. In this case, the above quasi-three-level energy diagram needs to be extended to have five levels.

1.8 Direct methods

Direct methods measure the amount of light that is absorbed nonlinearly as it passes through a material. Such methods are typically applied to the measurement of MPA cross sections, although often information regarding the order of the MPA process can be obtained as well. Direct measurement of MPA cross sections can be challenging, because the MPA is so weak that only a small fraction of the incident photons is absorbed. High incident power is generally required to produce a measurable nonlinear signal. However, such high laser irradiance may cause unwanted phenomena to occur, such as ESA. These effects can in turn complicate the interpretation of measurements. Some of these methods will be presented below and the interest will be focused on Z-scan technique, which is the direct method that 2-BIT experimental results will be compared to.

1.8.1 Transmission as a Function of Laser Irradiance[4][15]

One of the first approaches used for the determination of MPA coefficients was the nonlinear transmission (NLT) method, which entails determining the transmission, *T*, of a sample as a function of the incident peak irradiance Imax (0).The technique relies on measuring, as a function of irradiance, the attenuation of a collimated beam that propagates through a multiphoton absorbing medium.
NLT technique is both simple in concept and relatively straightforward to implement. NLT also has a number of advantages that stem from its use of a collimated laser beam. In particular, issues such as self-focusing, white-light generation, higher-order nonlinear excitation, and material damage are typically not a problem in NLT measurements, in contrast to the situation for techniques requiring focused beam geometry. One of the biggest drawbacks of NLT measurements is that any nonlinear absorption process can contribute to the signal, and it is not easily possible to distinguish among different mechanisms (e.g. ESA) or different orders of nonlinearity that are present simultaneously.

1.8.2 Loss Modulation[16]

Loss modulation is a technique that is used in order to detect a weak MPA signal. In this method, a train of femtosecond pulses from an oscillator is modulated sinusoidally by a pair of acousto-optic modulators. The beam is focused in a sample

and the transmitted intensity is detected. MPA gives rise to a signal at twice the modulation frequency. A lock-in amplifier can be used to separate the desired signal from those at other frequencies with high selectivity.
As the power that is absorbed via an MPA process (*PMPA*) is proportional to the input power raised to the power of the number of photons absorbed (*n*), i.e. $P_{MPA} \propto \sigma_n P^n$, the greatest MPA occurs at the peaks of the sinusoidal modulation.

One of the advantages of loss modulation is its high sensitivity as compared to other direct methods. Furthermore, much lower power/irradiance is required to measure an absorptive nonlinearity with loss modulation than with other direct methods. However, to perform loss modulation with high sensitivity the experimental setup requires the use of two modulators.[16] Careful alignment is also required so that the two combined beams overlap both spatially and temporally to yield an optimal combined beam. Moreover, as with other direct methods, loss modulation data must be obtained over a wide range of input powers if there are contributions from multiple absorptive nonlinearities.

1.8.3 Z-scan technique

The most well-known method for measuring nonlinear absorption (and refraction) is the Z-scan technique, which was introduced by Sheik-Bahae et al. in 1990**.** [17]A major advantage of the Z-scan technique is that it allows for the simultaneous determination of the magnitude and sign of nonlinear refraction and absorption in a single measurement using only one beam. A typical Z-scan experiment (**Figure 5**) relies on the direct measurement of the transmittance, T, of a sample as it moves along the propagation direction of a focused laser beam (which is denoted the z axis). The moving sample thus experiences a continuously varying irradiance at each different z position.

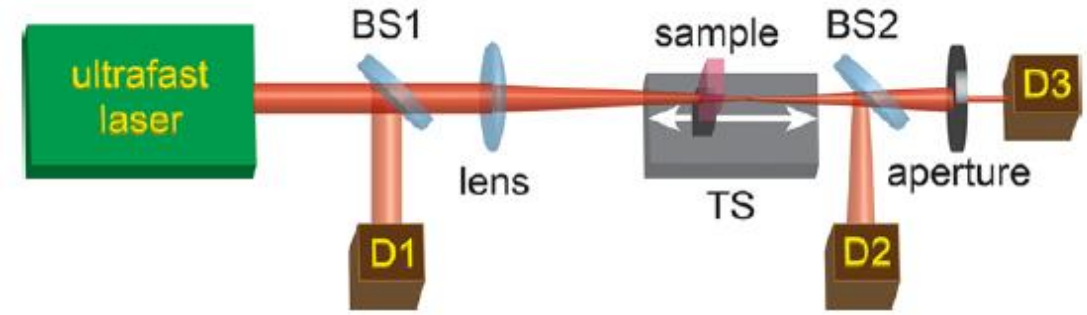

Fig.5 *Schematic of a Z-scan set-up, which can be used for measurements of nonlinear absorption and refraction. BS1, BS2: beamsplitters; D1, D2 and D3: detectors; TS: translation stage.[Taken from* [6]*]*

The measurement of the transmission is typically performed in one or both of two different ways: either just after the sample, in which case the entire transmitted laser light is collected and measured, or after passing through a small aperture that is placed

in the far field. The former method is called an *"open aperture" Z-scan*, and is used to measure nonlinear absorption. The latter method is called a *"closed-aperture" Z-scan*, and is used to measure the nonlinear refraction.

Following the approach of Sheik-Bahae et al.[17] method and assuming cubic nonlinearity and square pulses, for small phase distortions ($|\Delta\Phi_0| < 1$) and small aperture ($S \cong 0$) placed in the far field, the expression for the transmittance is given by:

$$T(x) \cong 1 - \frac{4\Delta\Phi_0 x}{(x^2+9)(x^2+1)} \qquad (32)$$

Where the phase distortion is $\Delta\Phi_0 = k\gamma' I_0(t)\, l_{eff,}$ $k=2\pi/\lambda$, γ' the nonlinear refraction parameter, $l_{eff} = [1-\exp(-\alpha^{(1)} l)]/\alpha^{(1)}$ with l denoting the physical length of the sample and $x=z/Z_R$ is the Rayleigh length.

In **Fig. 6** two representative "closed-aperture" curves are shown. For the positive $\Delta\Phi_0$ value, the normalized transmittance shows a "valley-peak" feature, indicating positive refractive nonlinearity. In other words, the sample in this case acts as a positive (focusing) lens. On the other hand, for the negative $\Delta\Phi_0$ value, the obtained curve exhibits a "peak-valley" trace, indicating negative refractive nonlinearity (i.e., a defocusing lens).

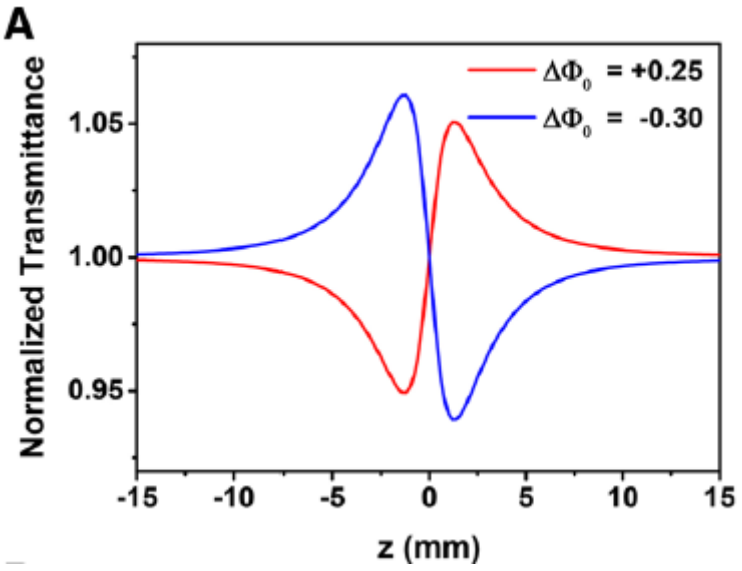

Fig. 6

The final expression for the nonlinear refractive parameter is:

$$\mathrm{Re}\chi^{(3)}_{xxxx}(\mathrm{esu}) = 10^{-7} n_0^2 c\, \gamma'/(48\pi^2) \qquad (33)$$

The measurement of nonlinear absorption is accomplished by removing the aperture (i.e., $S = 1$). In this case, it can be shown that the magnitude of $\alpha^{(2)}$ can be determined by fitting the obtained curve to

$$T(z, S = 1) = \frac{1}{\sqrt{\pi} q_0(z,0)} \int_{-\infty}^{+\infty} \ln\left[1 + q_0(z,0) e^{-\mu^2}\right] d\mu \qquad (34)$$

Where

$$q_0(z,0) = \frac{\alpha^{(2)} I_0 L_{eff}}{1 + \frac{z^2}{z_R^2}} = \frac{q_{00}}{1 + \frac{z^2}{z_R^2}} \qquad (35)$$

For $|q_0| < 1$, the above integral can be expressed in terms of a summation that is more convenient for numerical evaluation:

$$T = \sum_{m=0}^{\infty} \frac{[-q_0]^m}{(m+1)^{3/2}} \qquad (36)$$

In **Figure 7**, two representative "open-aperture" curves are shown obtained with the above equation using different q_{00}

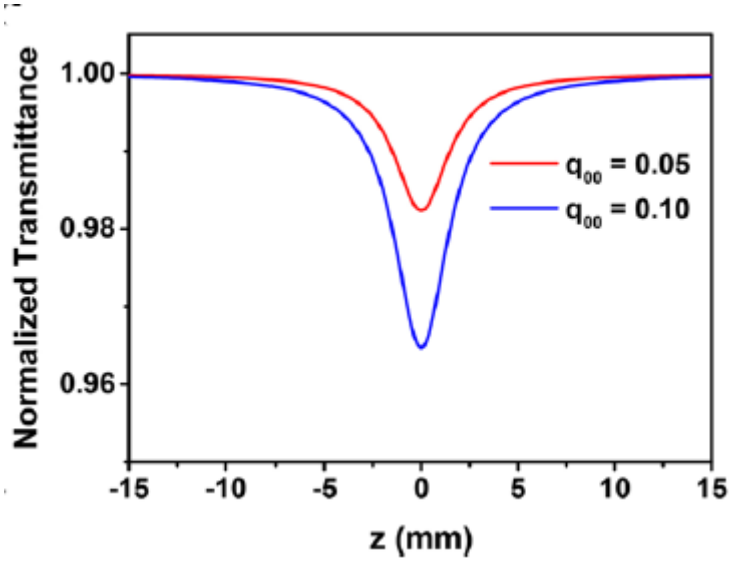

Fig. 7

In addition, the presence of a transmittance minimum or maximum in the "open-aperture" Z-scan recording indicates the sign of $\alpha^{(2)}$. A transmittance minimum implies positive $\alpha^{(2)}$ which is indicative of 2PA, whereas a transmittance maximum indicates negative $\alpha^{(2)}$.

With $\alpha^{(2)}$ having been determined from Eq. (36), the imaginary part of the third-order susceptibility, $\mathrm{Im}\chi^{(3)}$, can be calculated using Eq.(8).

Although the Z-scan is a relatively simple technique that allows for the separation of absorptive and refractive nonlinearities, it has some drawbacks and will be presented below.

- The beam size in the sample varies during the measurement; heterogeneities in samples can give rise to severe linear scattering, so Z-scan measurements require samples of high optical quality.
- Focused-beam geometry is used for Z-scan measurements, so the pulse energies must be tens of microjoules or even nanojoules, depending on the pulse width. However, focusing an ultrafast Gaussian beam can cause unwanted phenomena to occur.
- A Z-scan measurement is sensitive to all nonlinear absorption mechanisms, including 2PA, ESA and other processes that are present and contribute to the measured signal, such as thermal/cumulative effects.

Therefore, a number of approaches have been used to overcome some of these disadvantages in order to reduce the induction of extra nonlinearities.
One method for distinguishing between ESA and MPA was to use different pulse durations during the measurement. If Z-scan recordings taken with the same average irradiance but different pulse widths show no variation, then ESA is the predominant mechanism of nonlinear absorption. On the other hand, if Z-scan traces that are obtained at the same maximum irradiance are identical for different pulse widths, then MPA is the dominant mechanism of nonlinear absorption.
In order to be able to separate the pure electronic contributions from thermo-optical effects, variations of the Z-scan technique have been developed. One such technique involves a combination of the single-beam Z-scan technique with the thermal lens technique, in which a mechanical chopper is introduced to control the exposure time of the sample by means of a default chopping frequency and a chopper opening rise time.

1.8.4 Spectrally-Resolved, Two-Beam Coupling[18]

The spectrally-resolved, two-beam coupling technique introduced by Kang et al. can be used to determine the magnitudes and signs of nonlinear refraction and 2PA**.[99]** This technique relies on nonlinearity creating coupling between a pump pulse and a probe pulse. An intense pump beam induces a phase change and energy loss through cross-phase modulation and 2PA, respectively, leading to a variation in the transmission of a spectrally distinct probe beam.

1.9 Indirect Methods

Indirect methods rely on an observable other than optical loss as a proxy for the measurement of MPA. Many indirect methods offer the advantage of having zero background, which can make indirect techniques much more sensitive than direct

ones. However, because such techniques do not measure MPA directly, what is observed in an indirect measurement is an action cross section.

1.9.1 Nonlinear Fluorescence Excitation[19]

NFE has probably been the most widely used method of determining MPA cross sections. In this type of measurement**,** a fluorophore is excited via MPA. The molecule initially relaxes nonradiatively to the lowest vibrational level of the first excited singlet state, after which it fluoresces back to the ground state. The fluorescence emission intensity is proportional to the population of the first excited singlet state. The population of this state is, in turn, proportional to $I_{max}{}^{n}$, where n is the order of the nonlinear absorption process. A typical experimental apparatus for measuring MPA-induced fluorescence is shown in **Figure 8**.

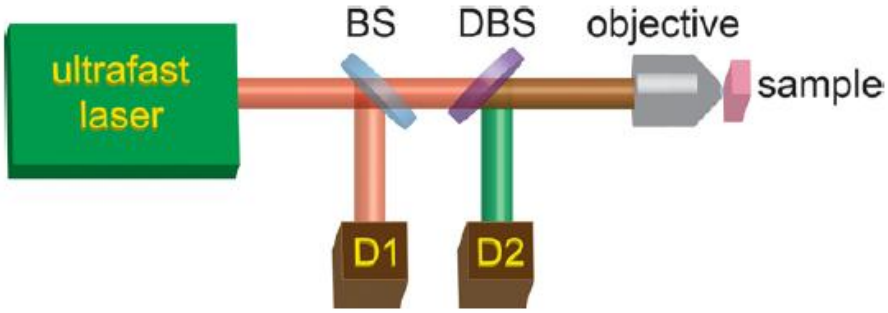

Fig. 8

NFE provides a good example of the difference between the direct measurement of an MPA cross section and the measurement of an action cross section, as the unknown parameter of σ_2 is measured through the product of the NFE experiment.

An important advantage of NFE is its high sensitivity, which allows for the measurement of higher-order nonlinearities with high accuracy, especially after taking into consideration the fact that direct measurements of MPA are not always easy due to the low absorption probability.
However, NFE also has a number of disadvantages. For example, the measurement needs to be performed at excitation irradiances that span several orders of magnitude to obtain a reliable exponent. However, as the irradiance increases many other factors can become important, such as stimulated emission, ESA and higher-order nonlinear absorption. All of these factors can result in significant deviations from the expected n^{th}– order power dependence of the integrated fluorescence intensity. The benefit in this case is that such deviations can assist in the identification of the other processes involved that compete with 2PA, such as stimulated emission and Raman scattering**.**[20]

1.9.2 Thermal Lensing

The thermal lensing effect was first reported by Gordon et al. in 1964.[21] Subsequently, this phenomenon has been applied as a spectrometric technique for measuring weak absorption coefficients, thermo-optical parameters and MPA orders and cross sections.[22] A thermal lens (TL) is formed in a material when a temperature increase is created by the non-radiative relaxation processes that follow optical absorption.[23] The change in temperature induces small changes in the refractive index of the medium that are a function of the laser intensity distribution. In the case of MPA, these changes in refractive index depend on properties such as the characteristics of the beam, the MPA cross section of the material, and the thermal properties of the medium (e.g., thermal diffusivity and conductivity).

In the most common implementation of the TL technique for measuring nonlinear absorption, a Gaussian pump beam is focused into an absorbing material, inducing a refractive index gradient. A probe beam, of much lower power, is distorted as it passes through the TL induced by the pump beam. By measuring the induced modification in the profile of the probe beam in the far field, the nonlinear absorption can be measured.

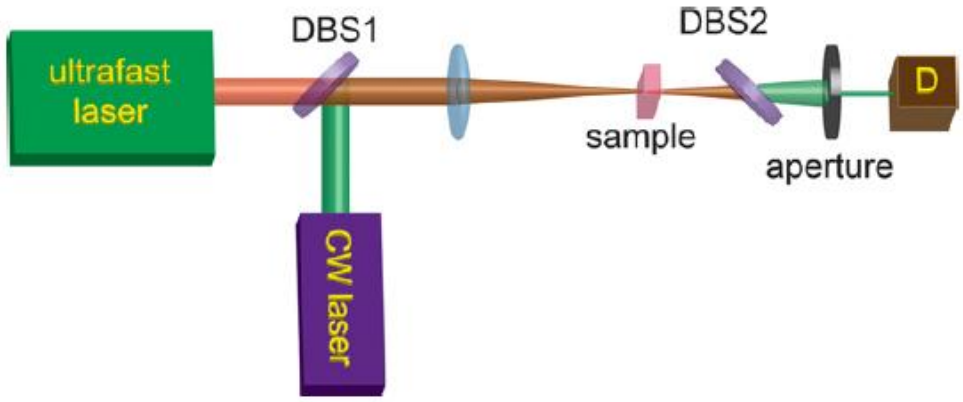

Fig. 9 *Schematic diagram of a dual-beam TL experimental setup for measuring MPA cross sections. DBS1 and DBS2: dichroic beamsplitters.*

The TL technique shares a drawback with many other techniques for the measurement of absorptive optical nonlinearities, which is that processes such as ESA, free carrier absorption, Raman scattering, and higher-order absorption can also contribute to the signal. As is the case in other methods, one of the best ways of ascertaining the presence of competing processes is to perform measurements over as broad a range of pump intensities as possible.

1.9.3 Effective Absorptive Nonlinearities in Multiphoton Photoresists

The information that MAP is able to give is still not enough as the nonlinear polymerization cross section does not always reflect the nonlinear absorption cross section like some of direct methods (i.e. NFE)[24]. Indeed, it has been found that the order of the effective nonlinear optical absorption for MAP at a given wavelength, i.e. the nonlinear absorption that leads to polymerization, need not match the dominant order of nonlinear absorption at the same wavelength. In order to indicate and correct this issue, some methods and techniques were developed.

One of the techniques was used, is the measurement of the width of the photopolymerized features as a function of fabrication velocity for a range of different average laser powers. To determine the order of the nonlinearity, we fit the data (line width vs. speed^{-1}) to the equation below.

$$V=A\,[1-\exp(-Bt)] \qquad (37)$$

Where V is the voxel volume, t is the dwell time (inverse scan speed) and A, B fitting parameters that their product gives the growth rate R_p.

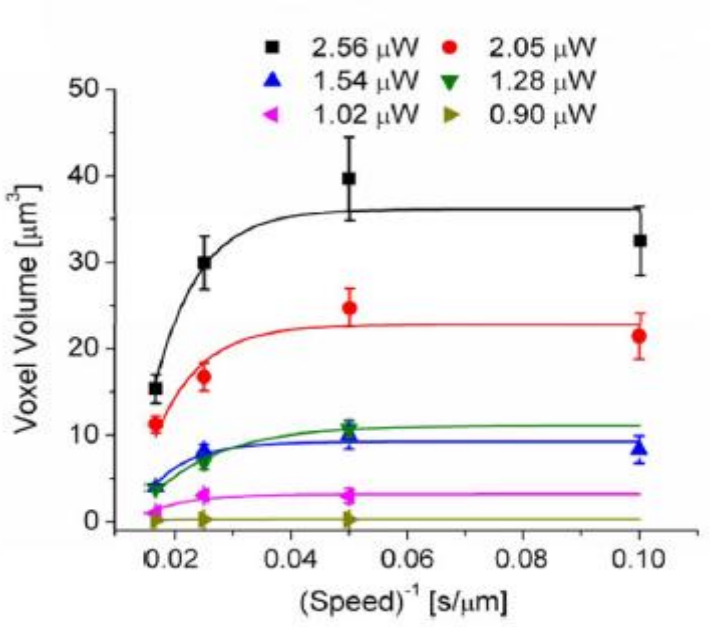

Fig. 10 Calculated voxel volumes as a function of inverse scan speed for different excitation powers.

The growth rate values corresponding to the data in Fig. 10 are plotted as a function of the average excitation power in **Figure 11**. The rate of polymer growth is expected to be proportional to $I_{max}^{\ n/2}$. By fitting the data in Fig. 11 with an expression of the form:

$$R_p = K|P - P_{th}|^{n/2} \qquad (38)$$

where K is a constant, P is the average power, and P_{th} is the threshold power for polymerization.

In this technique however, is necessary that the sample be developed and then inspected by scanning electron microscopy (SEM). In this occasion, development can cause shrinkage that is dependent on the degree of the exposure of the photoresist and coating and imagine by SEM can cause extra shrinkage. Another disadvantage of this technique is that the exposure time needs to be varied over a wide range. Also, the dependence of the local heating on velocity may confound the determination of n[24].

Another technique for determining the effective nonlinearity in multiphoton photoresists is measuring the exposure threshold as a function of pulse energy at different pulse repetition rates.[25] This method can provide detailed information on the processes that contribute to MAP at different peak irradiances, and is based on the fact that the exposure per pulse required reaching the insolubility threshold decreases with increasing repetition rate. For an *n*-photon process, the accumulated exposure dose D_{acc} for a single voxel is given by:

$$D_{acc} = N_p D_p \propto R E_p^n \qquad (40)$$

where N_p is the number of incident pulses, D_p is the exposure dose of a single laser pulse, R is the repetition rate, E_p is the pulse energy, and n is the order of the nonlinear absorption. Based on this equation, the threshold pulse energy (E_{th}) needed to reach the threshold dose ($D_{acc} = D_{th}$) for polymerization is given by:

$$E_{th} \propto (D_{th}/R)^{1/n} \qquad (41)$$

A similar approach was introduced more recently, in which the effective order of nonlinear absorption is determined by measuring the polymerization threshold at a fixed repetition rate but different exposure times.[26]

Both of these techniques can provide reliable and accurate measurements of the order of effective nonlinear absorption in multiphoton photoresists, which in principle may involve a combination of multi- and single-photon absorption steps that drive population to the state from which chemistry takes place. However, both of these techniques require fast, nonmechanical shutters and high-power oscillators, which are not available in many laboratories in which MAP is performed.

The latest technique that was produced in order to measure the order of the effective nonlinear absorption in photoresists is the Two-beam Initiation Threshold (2-BIT) technique. This technique is going to be presented extensively in the next chapters.

Chapter 2

A simple and complementary method will now be introduced for determining the effective order of nonlinear absorption processes in photoresists. The 2-beam initiation threshold (2-BIT) technique can be implemented with the addition of a few simple optics, can be performed with a single, low-power ultrafast oscillator, and allows for the determination of the order of the effective nonlinear absorption using only a single repetition rate.[1][6]

2-BIT technique measures the order of the effective nonlinear absorption in negative-tone photoresists, as in every MAP[27] method. Negative-tone photoresists (**Figure 11**) is a type of photoresist in which the portion of the photoresist that is exposed to light becomes insoluble to the photoresist developer. Specifically, photoresists have highly nonlinear exposure curves, such that they become insoluble above a threshold exposure dose.

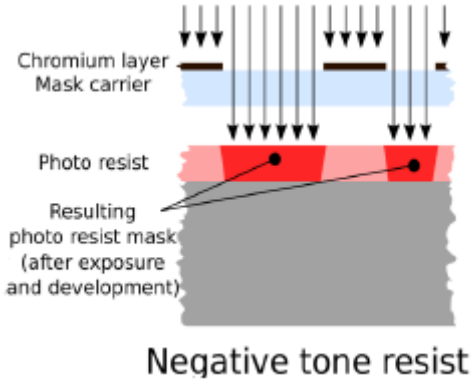

Figure 11 *Visual example of negative photoresist*

Before we describe the experimental set-up for the 2-BIT technique, it is essential to interpret the reasons why we use two beams instead of one single beam. So, in MAP we need ultrafast pulses. However, this can bring other time scales into play. First of all, ultrafast pulses are typically much shorter than the time scales on which photoinitiators undergo photochemistry**.** Secondly, due to the small size of the region irradiated at any given time in MAP[27], the diffusion of heat or species such as radicals or quenchers can play an important role in determining the threshold exposure. Diffusive effects leading to termination become important when, due either to a low pulse intensity or a low repetition rate, the exposure time at a given spot is relatively long **.** These effects are the reason why it is necessary to determine the order of the effective nonlinear absorption of a photoresist at a fixed repetition rate.[28]

If the exposure conditions are comfortably between the two parameters above, then overcoming the exposure threshold can be equated with generating a specific density of photoinitiators that have been excited at some time in the exposure window. It is essential that the repetition time be much longer than the excited state lifetime of the photoinitiator, to prevent any effects of excited-state absorption. Typical radical photoinitiators generate radicals on a 100 ps time scale, which is 2 orders of magnitude faster than a typical repetition rate. The radicals that are formed do not absorb the laser light, and so are unaffected by subsequent pulses.[29]

It is also important that the repetition period is much shorter than the termination time scale, so that the effects of the laser pulses are cumulative. In a typical photoresist, termination becomes important on time scales of 100μs or more , which is much longer than the typical dwell time on a given spot.

2.1 Experimental Setup

In order to exploit the capabilities of this technique, an experimental set up was developed. The oscillator that was used is a Femtolasers Fusion Ti: Sapphire Diode-Pumped femtosecond laser (wavelength 800nm) with integrated dispersive mirrors that pre-compensate the beam delivery and focusing optics to achieve sub-20fs duration pulses into the sample. The repetition rate of the laser was 75MHz and 450mW as maximum output power.

As the **Figure 12** indicates, before the beam is separated in two parts, it passes through a lens with focal distance 160cm in order to be collimated and reduce the divergence. Then, the beam is sent to a beam splitter (70/30) and is being split into two parts. Because the beam splitter does not separate the beam into two equal parts, we also used a half-wave plate so that each beam has the same energy with the other. The average power of each beam was adjusted using a half-wave plate and Glan-Taylor polarizer.

The two beams were combined through a polarizing beam cube and made collinear. Before the beams get together, we made sure that the length of both beam paths were adjusted so that the consecutive pulses arrived at the sample with roughly equally spaced timings, giving an effective repetition rate of 150 MHz . The timing between the pulse trains was adjusted using a fast photodiode and an oscilloscope.

After combining the two beams, they pass through an attenuator that is being used in order to find the power thresholds that polymerization occurs. The beams were sent through telescope and were focused into the photopolymerizable composite using a high numerical aperture focusing microscope oil-immersion objective lens (100x, N.A. = 1.4, Zeiss, Plan Apochromat), the back aperture of which was overfilled. Samples were mounted on a 3-axis piezoelectric stage for fine sample positioning in

all dimensions. The piezo stage was attached to a motor-driven stage for coarse sample positioning. The movement of the sample stage was controlled using 3Dpoli software, and fabrication was followed in real time using a CCD camera. The average power used for the fabrication was measured before the objective.

Special attention was paid to ensure that the two beams had exactly the same diameter and divergence at the entrance pupil of the objective, such that beams of the same average power would also have the same on-axis intensity.

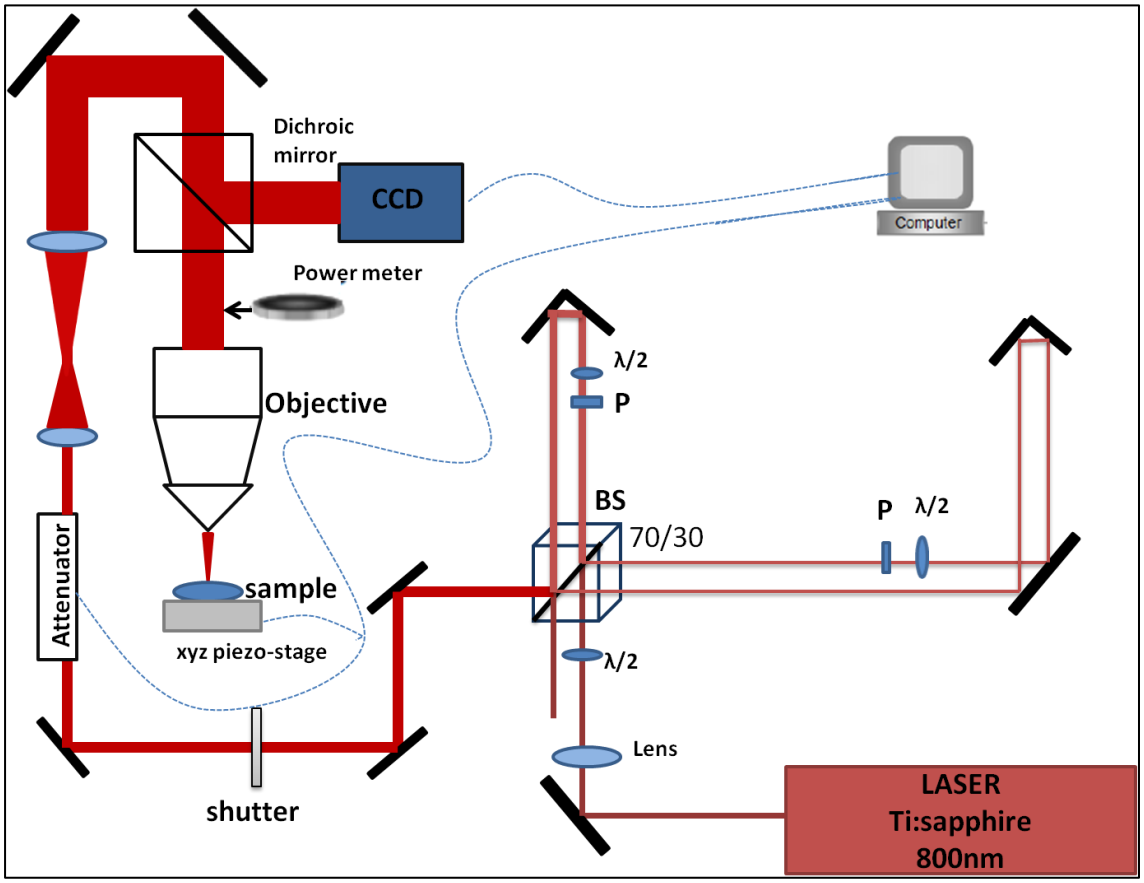

Figure 12 *2-BIT Experimental set-up*

The repetition rate of laser is 75MHz, so when the output beam is divided into two beams the repetition rate of each beam is again 75MHz. When the beams are combined after traversing their paths, the repetition rate is 150MHz. Concerning the repetition time between the two beams and the repetition period of each beam, it depends on the length of each beam. It is essential that the repetition time must be much longer than the excited –state lifetime of the photoinitiator (100 ps) in order to prevent ESA and the repetition period must be shorter than the termination time scale (100μs), so that the effects of the laser pulses are cumulative.

In order to achieve these to extremes, the length of the one beam path must be longer that the other beam path. Specifically, the difference between the lengths of each beam path was calculated to be 197cm.

Also, the repetition time and period was calculated as it is shown below.

Repetition time: $T_1=1/f_1$ where $f_1= 150* 10^6$ Hz → $T_1= 6.67$ns

Repetition period: $T_2=1/f_2$ where $f_2= 75 * 10^6$ Hz → $T_2=13.3$ns

In Figure 12 is presented the way both beams reach the sample.

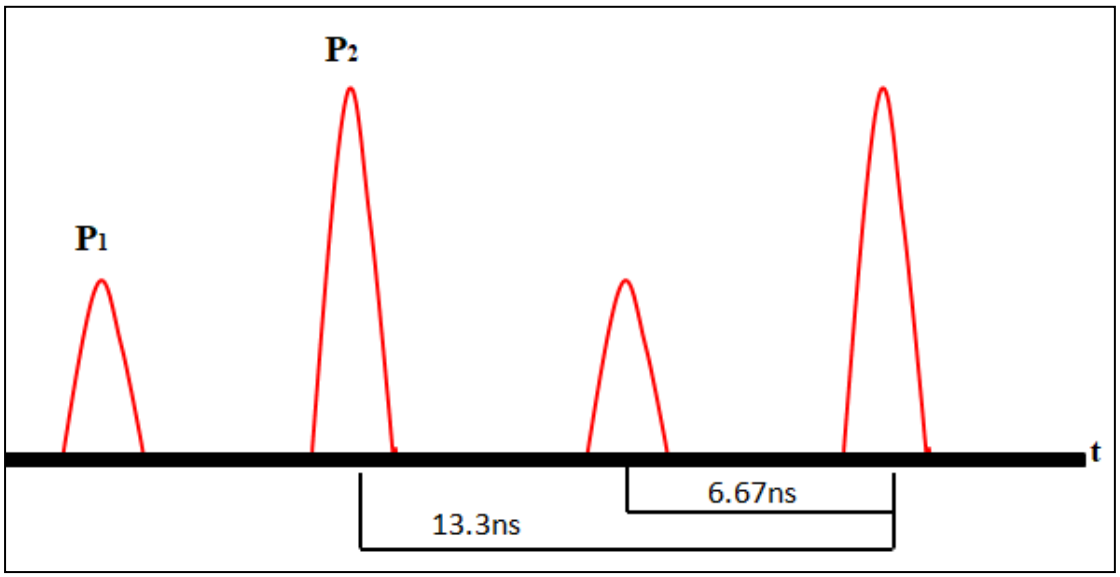

Figure 13

2.2 Experimental methodology

As was mentioned above, in the 2BIT method during the measurement, two beams are used. In order to perform the experiment, it is essential to determine the threshold power for each beam.

The threshold power, is the minimum average power for which crosslinking is observed, can be defined as $P_{th}\ (t_w, v_{pulse})$, where t_w is the fixed duration for the exposure window and v_{pulse} is the fixed repetition rate for the ultrafast pulses.

In 2-BIT technique two beams are used. So for the case in which exposure occurs via two independent trains of pulses that are identical in wavelength, duration, and repetition rate, but not in intensity. For simplicity, assume that these pulse trains are

timed such that pulses arrive at the sample at repetition rate $2\nu_{pulse}$. So long as ν_{pulse} and $2\nu_{pulse}$ are:

(1) small enough that there is plenty of time for excited photoinitiators to undergo chemistry between pulses
(2) large enough that diffusive effects are unimportant between pulses

The exposure threshold will be reached when:

$$P_1^n + P_2^n = P_{th}^n \qquad (42)$$

Here, the subscript denotes the pulse train and n denotes the number of photons involved in the transition to the excited state that is the gateway to crosslinking. This equation can be recast in terms of normalized powers $\bar{P}i = P_i / P_{th}$ as:

$$\bar{P}_2 = \sqrt[n]{1 - \bar{P}_1^n} \qquad (43)$$

Thus, by measuring the value of $\bar{P}_2$ required to reach the threshold exposure for different values of $\bar{P}_1$, n can be determined directly. In practice, the power of each beam is normalized to the threshold power for polymerization using that beam, to correct for any minor differences in properties such as beam size, pulse length, or focal volume.

Specifically, before the measurements start, the threshold power for each beam is measured. In order to measure the threshold power for the first beam, the second beam is blocked. Then, through the 3D-poly program sets of lines were created, at a constant distance above the cover slip surface at a stage velocity of 20μm/s. The minimum average power at which fabricated lines were observed was then determined visually on the monitor. Although the threshold exposure measured may differ for different optical systems, the normalization procedure described above corrects for any such differences. For the threshold power of the second beam, the same procedure is followed.

Since the threshold powers of both beams are measured, the measurements procedure is as it follows. The power of the first laser beam was then lowered to a set of fixed values below the threshold. For each of the fixed values of P_1, the corresponding minimum value of the power of the second beam, P_2, for which polymerization was observed at the same stage velocity was determined. The values of $P1$ were chosen so that a representative range of values of P_2 was measured, such that the plot of $\bar{P}_2$ vs. $\bar{P}_1$ could be fit reliably. At least five measurements were made for each value of P_1 so that reproducibility could be quantified.

2.3 3D structure fabrication

The experimental setup employed for 3D structure fabrication has been described previously.[30, 31] A Ti: Sapphire femtosecond laser (Femtolasers Fusion, 800 nm, 75 MHz, <20 fs) was focused into the photopolymerizable composite using a high numerical aperture focusing microscope objective lens (100x, N.A. = 1.4, Zeiss, Plan Apochromat). Sample movement was achieved using piezoelectric and linear stages, for fine and step movement, respectively. The whole DLW setup was computer controlled using the 3DPoli software. [30][27]

Specifically, the beam path consists of various optical components, most important of which are the shutter, attenuator, dichroic mirror and the galvanometric mirror scanner (Galvo-scanner) or piezoelectric stages (Nano-cube). Through the attenuator, the energy/pulse can be adjusted, which is used to optimize the fabrication parameters. The energy/pulse is measured with the power meter. The shutter controls whether the beam incidents on the sample or not. Both shutter and attenuator are controlled via computer. The dichroic mirror reflects the incoming laser beam but allows the back-reflected portion from the sample to pass. This back-reflected portion of the beam is guided in the CCD camera, which is connected to the computer, for the online control of the fabrication procedure.
Figure 14 illustrates the beam path for the galvo-scanner. The same illustration can be applied on the nano-cube as well.

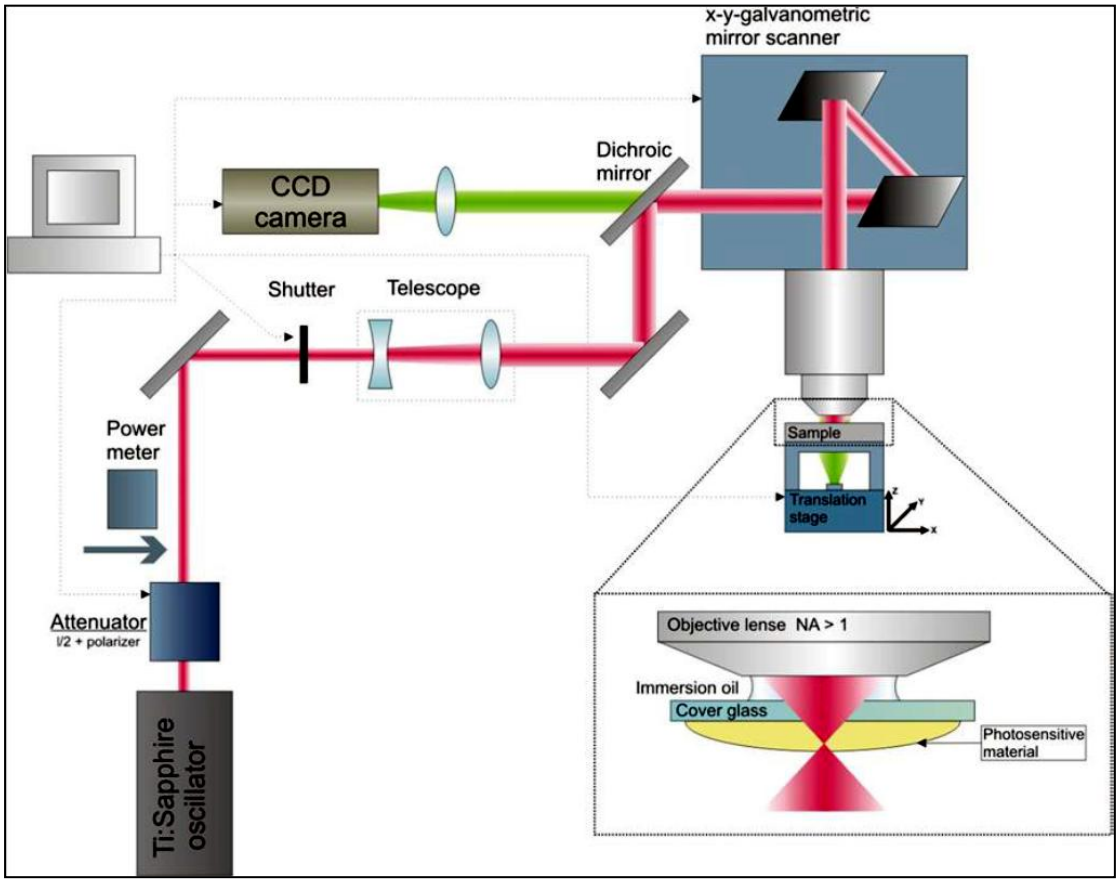

Figure 14 *Illustration of the setup for 2PP [Taken from* [31]*]*

2.4 Materials

The materials investigated in this work, are hybrid photosensitive materials that undergo Sol-Gel process in order to be synthesized. Such materials have the advantage of combining the dissimilar properties of the two components, in one system. The inorganic part of these composites is derived from metal alkoxides, which upon hydrolysis and condensation, form an inorganic network. The organic part comprises monomer units which carry photopolymerizable functional groups that are attached to the inorganic network. The photosensitivity of these materials arises from the use of appropriate photoinitiators. Such molecules, when treated with specific wavelength radiation, have the ability of initiating polymerization of the organic part, resulting in the formation of an organic-inorganic network. Sol-gel materials have been applied in many fields, such as membranes, chemical sensors and catalysis.

Sol-gel process can be viewed as two separate processes: Hydrolysis and Condensation [31]**.** Both reactions are affected by a variety of factors, most significant of which are, pH, temperature and, the nature and concentration of the catalyst used **[93].** The general reaction pattern is presented in Figure 14.

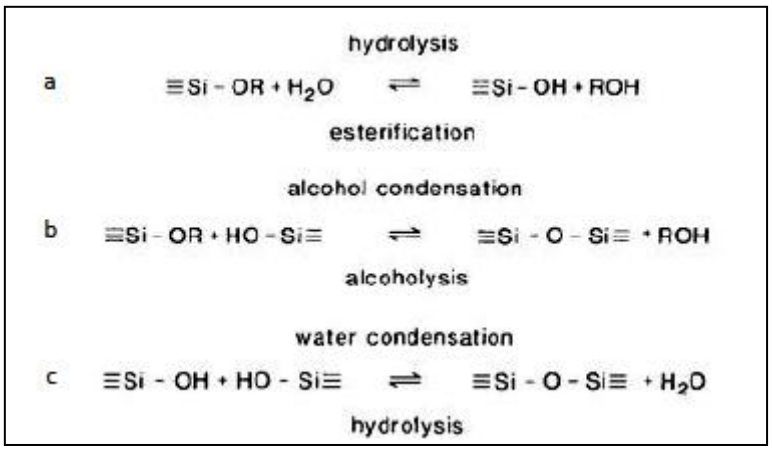

Figure 15 *General case of hydrolysis and condensation* **[93] .**

Hydrolysis is the reaction of an organic monomer with a water molecule (Figure 14a). The monomer is a silicon composite, where the R groups are carbon chains. Through this reaction, a hydrogen atom replaces an R group of a monomer. Hydrogen chloride (HCl) is used as a catalyst.

Condensation includes the products of hydrolysis. Monomers react with each other building large molecules that are bridged with one another. There are two ways condensation occurs. In alcohol condensation, one reacting monomer is hydrolyzed while the other is not (Figure 14b). In water condensation, both reacting monomers are hydrolyzed (Figure 14c). The by-product of each reaction is small alcohol or water molecules, respectively

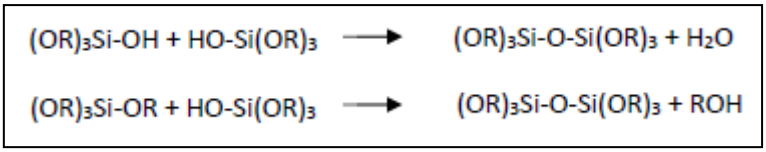

Figure 16 *Water condensation (top) and alcohol condensation (bottom).*

The ever-increasing water and alcohol concentration eventually "clog" the system, slowing down the condensation process. By drying at low temperature or low pressure, the trapped water and alcohol molecules, as well as the solvent, are removed from the network and the condensation can continue. This stage is called gelation and any significant volume loss occurs at this point. This concludes the sol-gel method.

2.4.1 Synthesis of Sol-Gel material

Recently this organic-inorganic hybrid sol-gel material, which is a zirconium-silicon composite (SZ8020), was produced by M. Farsari and M. Vamvakaki for photonic applications by multiphoton polymerization technique. The characteristic of this material is the minimal shrinkage during photopolymerization**.**

The hybrid materials have to fulfill certain characteristics. First it must be polymerizable and, second, photosensitive. These two requirements can be summarized in the term photopolymerizable.
In this work, two materials are used. Their production follows the same pattern. This pattern can be divided in four steps.

First, methacryloxypropyltrimethoxysilane (MAPTMS) and 0.1M of HCL diluted in water are combined in a flask. The process of hydrolysis and condensation initiates immediately. The solution is stirred for ~15mins to become homogeneous.

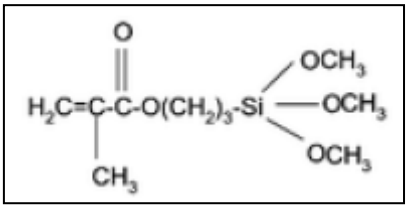

Figure 17 *Structural formula of MAPTMS*

Second, ZPO and an organic component, which in this occasion is MAA (methacrylic acid) are combined in a second flask. ZPO stands for zirconium propoxide. No reaction occurs between ZPO and MAA. Because ZPO reacts with moisture, it must not meet atmospheric air, so it stored in propanol in 70%w/w concentration. The organic component serves to protect ZPO from the humidity in the air. The solution is stirred for ~15mins to become homogeneous.

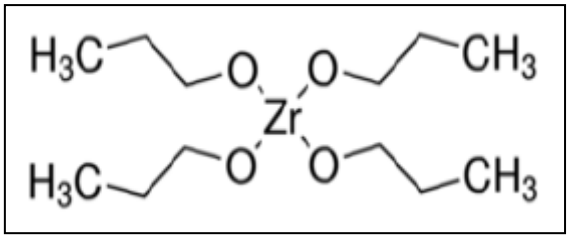

Figure 18 *Structural formula of ZPO*

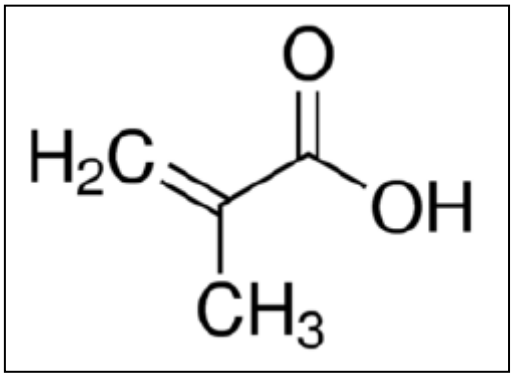

Figure 19 *Structural formula of MAA*

Third, the MAAPTMS solution is added to the ZPO. Zirconium joins the network of silicone. This will provide a mechanical sturdiness to the structures fabricated. The solution is, again, stirred for ~15mins to become homogeneous. Next, the photoinitiator, Bis, is added to the mixture at 1w% with respect to monomers. Bis stands for 4,4'-Bis(diethylamino)benzophenone and is completely soluble in the solution. Bis is chosen as photoinitiator because it absorbs effectively in close UV (~400nm) and non-effectively in close IR (~800nm).

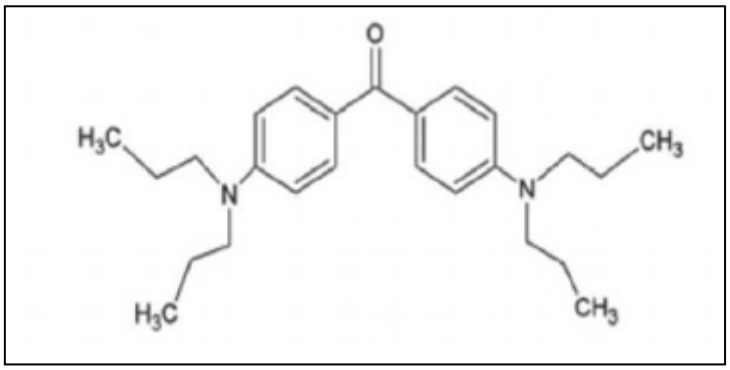

Figure 20 *Structural formula of Bis*

Fourth, the solution goes through a filtering process in which molecules larger than 0.22μm are filtered out. These large molecules can affect the fabricated structures. The material is complete.

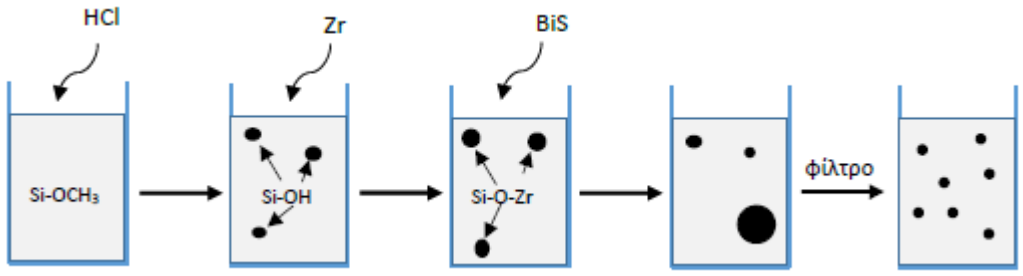

Figure 21 *Production of the hybrid material*

The ratios of mixture are:

$$\frac{n_{ZPO}}{n_{MAPTMS}} = \frac{2}{8} \qquad \text{and} \qquad \frac{n_{MAA}}{n_{ZPO}} = 1$$

The second sample was made with the same procedure, Sol-Gel but there are some differences in the materials that were used. Also, the photoinitiators in this material are synthesized at the lab of the Dr. Frederic Dumur.

Firstly, as the organic component that is mixed with ZPO is used DMAEMA. DMAEMA stands for 2-(Dimethylamino) ethyl methacrylate and its presence makes the fabricated structures softer. Secondly, the photoiniators that was used are given below:

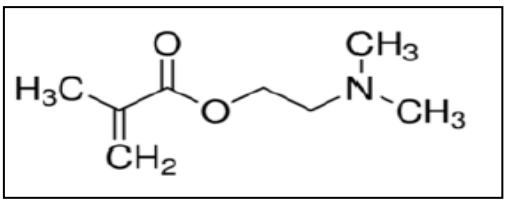

Figure 22 *Structural formula of DMAEMA*

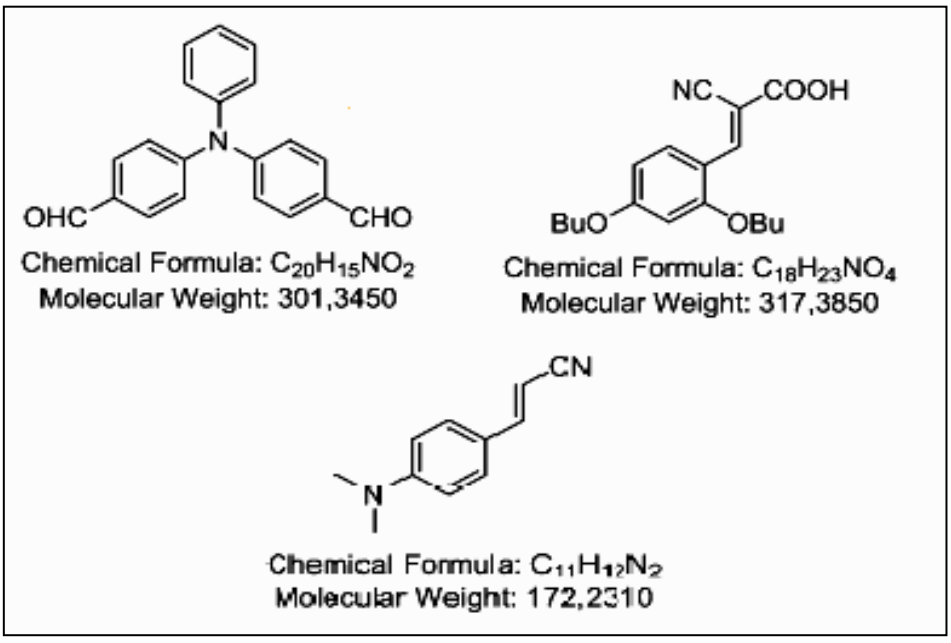

Figure 23 *Structural formula of Dr.FredericDumur's photoinitiators*

The ratios of mixture are:

$$\frac{n_{ZPO}}{n_{MAPTMS}} = \frac{3}{7} \quad \text{and} \quad \frac{n_{DMAEMA}}{n_{ZPO}+n_{MAPTMS}} = 30\%$$

2.4.2 Sample treatment

Samples are created by casting a drop of the material on a glass substrate. The glass substrate has undergone a specific treatment, so fabricated structures can attach on its surface during photopolymerization. This process aims to add MAPTMS monomers on the glass surface. First, the glass substrate is immersed in ethanol for 1 hour in the ultrasound machine. This serves to clean the surface. Second, the glass substrate is added in a 20mL of dichloromethane + 250μL of MAPTMS solution under ultrasounds for 4 hours. In this step, the MAPTMS chains are added on the surface. Now the glass substrate is ready to use. After some drops of the material are casted on the glass, the sample is either heated or placed under low vacuum conditions, overnight. This results in the gelation of the sol. The gelated sample goes under photopolymerization.

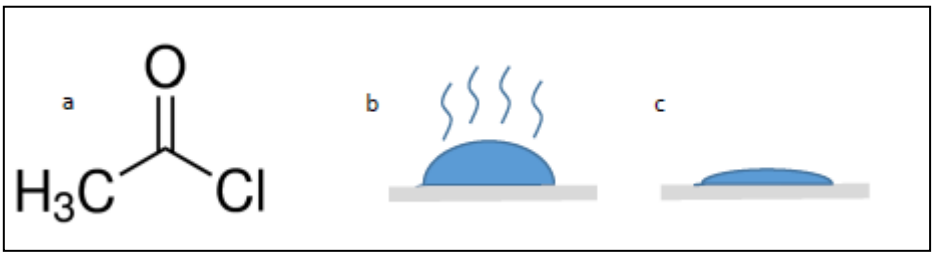

Figure 24 *a) Structural form of dichloromethane [Sigma Aldrich], b) Drop of material on glass substrate and gelation, c) Dried sample.*

Chapter 3

3.1 Results and Discussion

In this chapter, the results of this thesis will be presented. First of all, the linear absorption spectrums for each photoinitiator will be presented, as well as the 2-BIT measurements. A matrix with the experimental values of order of the effective nonlinear absorption for each photoinitiator will be introduced, as well.

3.2 UV-Vis and Emission measurements and 2-BIT results

The absorption spectrum of the 4, 4'-Bis (diethylamino)benzophenone that was obtained with the SZ8020 material has the same position on the absorption band as the one without the material. The photoinitiator 4, 4' Bis (diethylamino)benzophenone has an absorption peak at 373nm (**Figure 25a,b**)

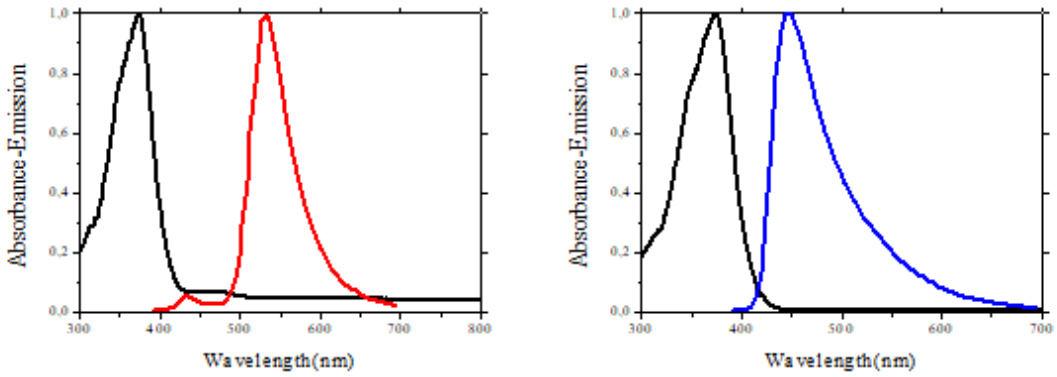

Figure 25 *a) SZ8020-Bis in 1-propanol b) Bis in DCM*

The best-fit exponential *n* was determined in each case by nonlinear fitting of the 2-BIT data to Eq. (43) as it seems in **Figure 26.**

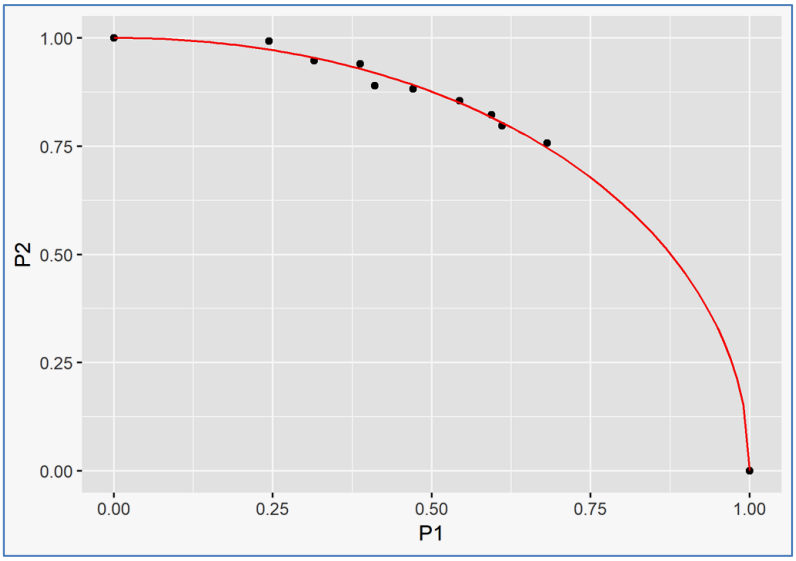

Figure 26 *2-BIT data for photoresist containing 1.0 wt% Bis*

The threshold power for each beam for Bis was P_1^{th}= 4.80mW and P_2^{th}=4.00mW and the best-fit exponent for the 2-BIT data is 2.06. Eventually, this material acts quadratically at 800 nm, as has been suggested reported **(paper bis zscan).**

Following, the results for the photoinitiators that where synthesized in Dr.Frederic Dumur's lab will be presented.

The photoinitiator $CH_{20}H_{15}NO_2$ has a strong absorption at 370nm, both when the spectrum was obtained with the solution with DMAEMA and without it. This absorption indicates that the n^{th} order of the effective nonlinear absorption should be quadratical.

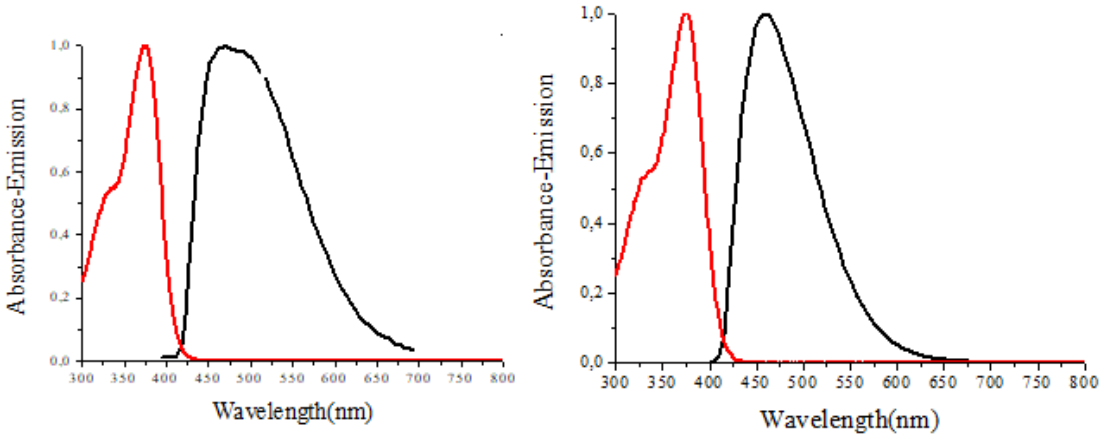

Figure 27

The best-fit exponential *n* was determined in each case by nonlinear fitting of the 2-BIT data to Eq. (43) as it seems in **Figure 28.**

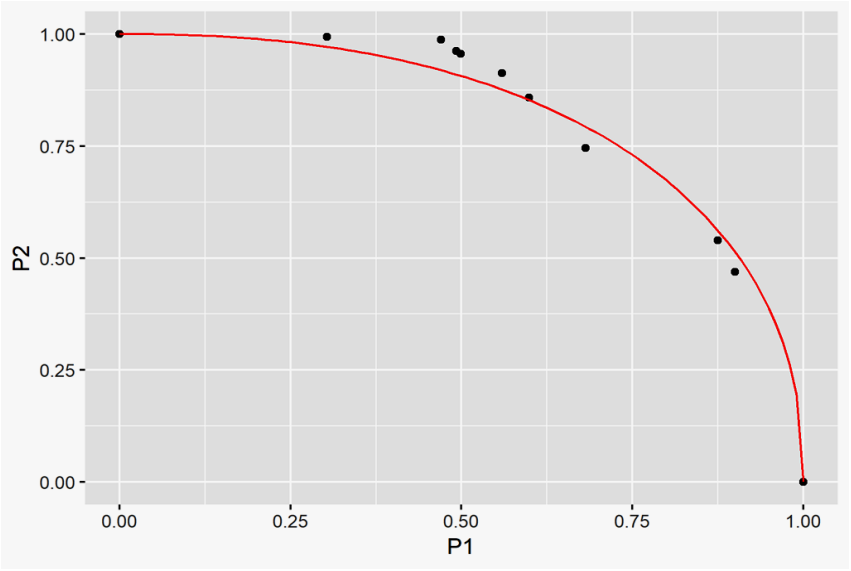

Figure 28 *2-BIT data for photoresist containing 1.0 wt%* $CH_{20}H_{15}NO_2$

The threshold power for each beam for $CH_{20}H_{15}NO_2$ was P_1^{th}= 2.00 mW and P_2^{th}=1.60mW and the best-fit exponent for the 2-BIT data is 2.30.

$CH_{18}H_{23}NO_4$ is another lab synthesized initiator. The 2-BIT data for this initiator are shown in **Figure 30** for excitation at a wavelength of 374 nm (**Figure 29**). The single-beam threshold power for each beam was P_1^{th}= 14.75 mW and P_2^{th}=10.80mW, and the best fit exponent for the 2-BIT data is 1.71, indicating that polymerization is a 2-photon process for this initiator at this wavelength.

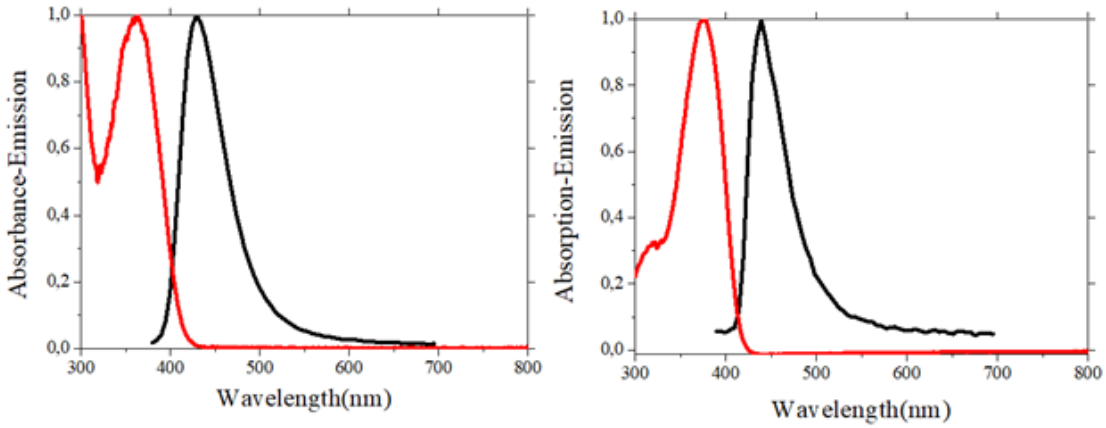

Figure 29

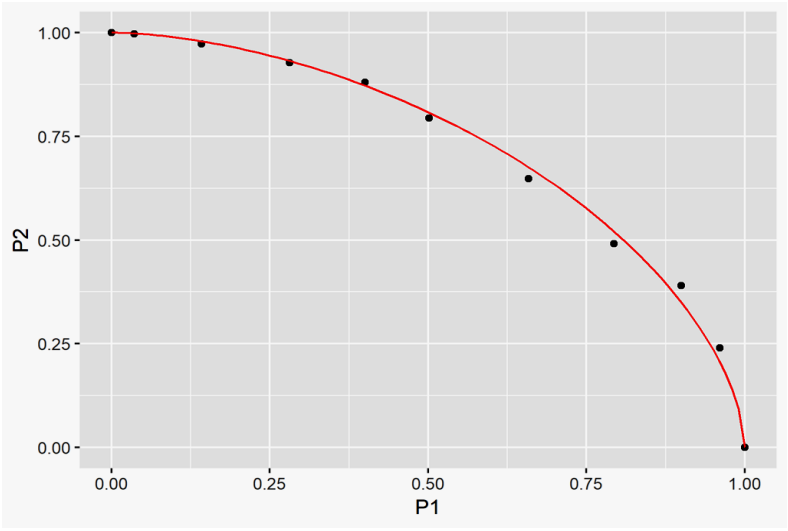

Figure 30 *2-BIT data for photoresist containing 1.0 wt%* pi2

The last photoinitiator that was measured by the 2-BIT technique is PI3. The 2-BIT data for a photoresist containing this material for 800 nm excitation are shown in **Figure 31**. As can be seen from the absorption spectrum in the **Figure 32**, this material has peak absorption at 363nm. In this case, the threshold power for each beam was P_1^{th}= 3.05 mW and P_2^{th}=2.70mW. The 2-BIT data are best fit with an exponent of 1.66, indicating that the dominant effective nonlinear absorption is23-photon at 800 nm.

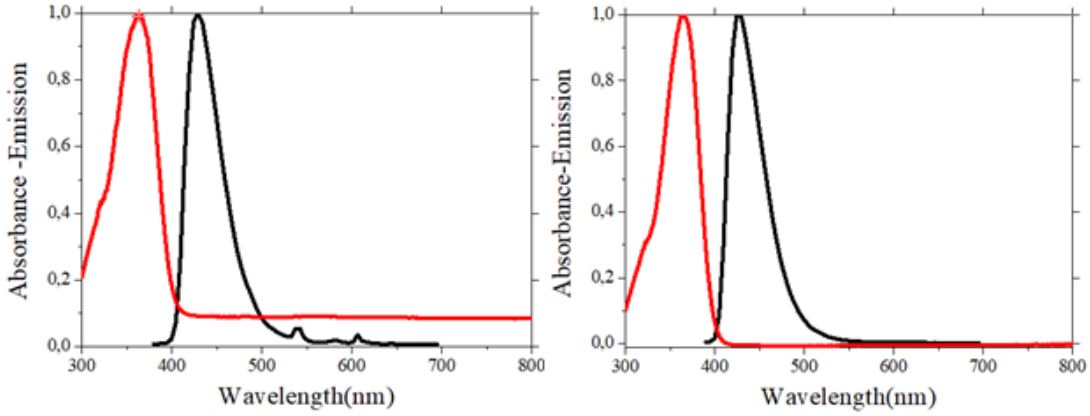

Figure 31

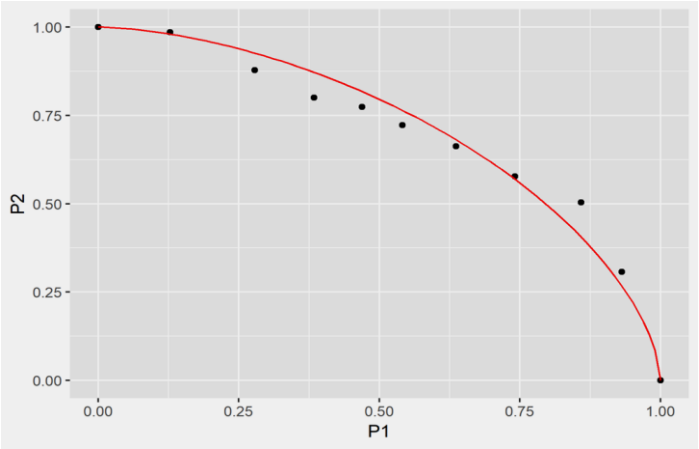

Figure 32

The results in brief are given in the table below.

Photoinitiator	n	P_1^{th}	P_2^{th}
1	2.30	2.00	1.60
2	1.71	14.75	10.80
3	1.66	3.05	2.70
4	2.06	4.80	4.00

In order to examine better the results of each photoinitiators, we made graphs that combine the theoretical 2PA and 3PA with our experimental results (**Figure 33**)

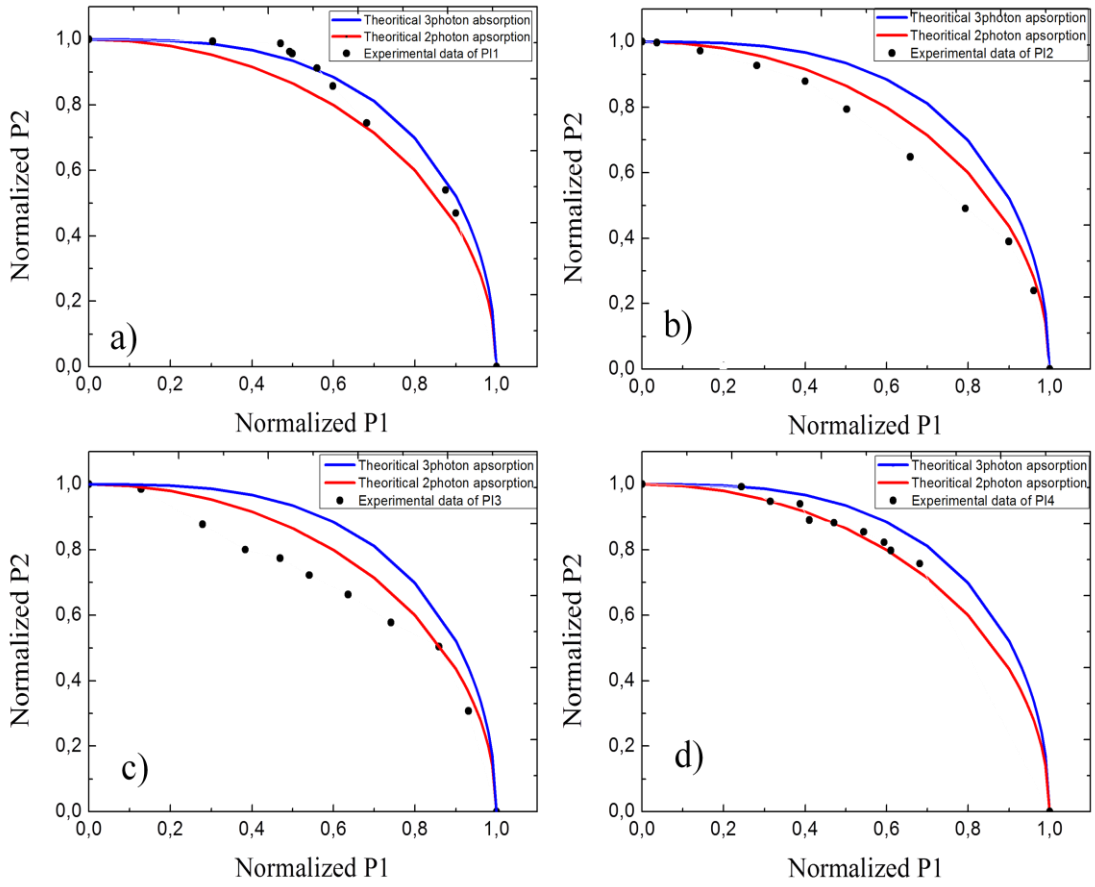

Figure 32 *a) Photoinitiator 1 b) Photoinitiator 2 c) Photoinitiator 3 d) Photoinitiator 4*

As we can observe from the graphs in Figure 32, the red and blue lines represent the theoretical graphs for 2PA and 3PA, corresponding. The black dots represent the experimental data for the 2-BIT technique. In **Figure 32a**, 2-BIT data are located between the 2PA and 3PA, confirming the result that n=2.30, which means that two or three photons caused the polymerization or some other nonlinear phenomena affect the final result. In **Figure 32b**, the experimental data from 2-BIT technique seem to be under the theoretical 2PA graph. In this case, the contribution of one or two photon resulted in the polymerization. The experimental data from 2-BIT technique of the photoinitiator 3(**Figure 32c**), are almost the same as the photoinitiator 2. Finally, the experimental data shown in **Figure 32d** indicate an unambiguous second order of nonlinear absorption. This result was expected as the photoinitiator 4 represent a commercial one that has been studied a lot of times in our lab.

3.3 3D STRUCTURES

In order to examine the resolution of the new lab synthesized photoinitiators, we fabricated some 3D structures. Specifically we fabricated such structures so that will be clear the range of the powers that the photoinitiator works. In **Figure 33** the 3D structures are given.

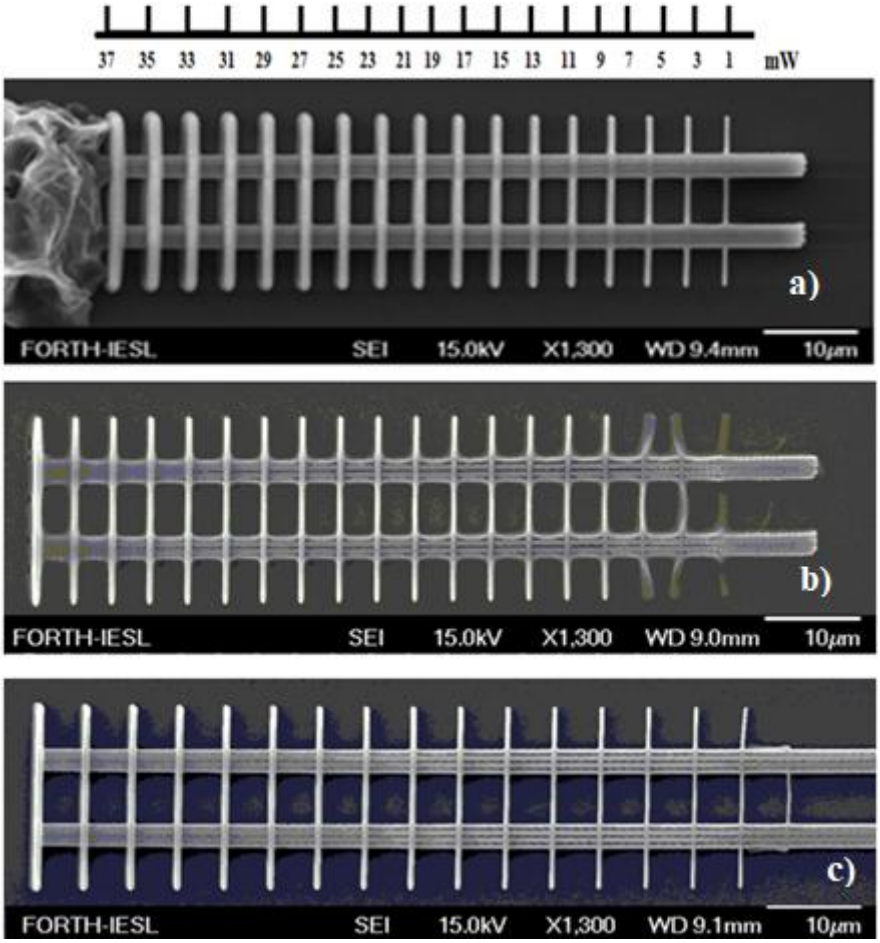

Figure 33 *a) Photoinitiator 1 b) Photoinitiator 2 c) Photoinitiator 3*

However, we had to determine the resolution of initiator, so we maximized one line (x40.000) and the resolution was found.(**Figure 34**)

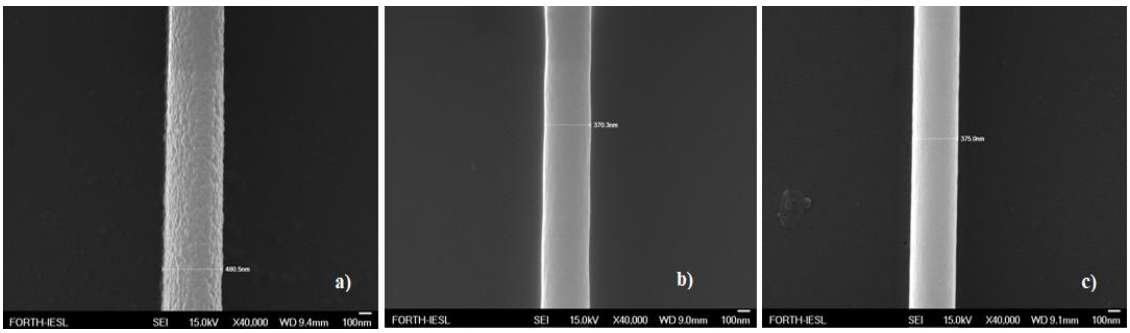

Figure 34 *a) Photoinitiator 1 b) Photoinitiator 2 c) Photoinitiator 3*

The resolution of the first photoinitiator is 480.5nm, for the second is 370.3nm and for the third one is 375nm.

3.4 Conclusion

2-BIT is a simple and effective method for the in situ measurement of the order of the effective nonlinear absorption in multiphoton photoresists, and as such can be an important element of the development of new materials that extend the capabilities of MAP. 2-BIT relies on the use of a single oscillator of fixed repetition rate, and so can be set up easily in virtually any laboratory in which MAP is performed.

This technique can be used with any type of MAP photoresist, and can be implemented with any of a wide range of means for determining the initiation threshold of a photoresist, including monitoring of lines or voxel during fabrication using optical or spectroscopic methods. 2-BIT allows the order of the effective nonlinear absorption of a photoresist to be determined without having to use devices for rapid beam modulation, and measurements can be performed at any desired repetition rate.

However, we have to remark on the fact that the order of the effective nonlinear absorption cannot be determined readily from the linear absorption spectrum alone. It is possible, for instance, that there is significant 2-photon absorption to the origin of the lowest singlet excited state in this molecule, but this state does not generate radicals this initiator does transition to initiating via 2-photon absorption.

Also, it is observed from the 2-BIT measurements that exponent *n,* for every photoinitiator studied, is non-integer. This fact could be arise from a combination of linear and 2-photon absorption. Another explanation for the non-integer exponent *n* could be that each pulse encounters some excited-state population left by the previous pulse, thus leading to ESA. The phenomenon of ESA is possible to contribute to the total nonlinear absorption.

In order to examine the resolution of the photoinitiators we create some 3D nanostructures. Specifically, we create structures that consist of lines that have been made with different powers. This fact encounters in the optimization of the determination of the polymerization threshold of the photoinitiators and the burn point.

In a future work, variations of 2-BIT technique can be used to make in situ measurements of the order of the effective optical nonlinearity (and therefore the multiphoton action cross section, as opposed to the multiphoton absorption cross section) not just in photoresists, but in any sort of system in which nonlinear absorption causes a property to reach a measureable threshold. With knowledge of the other relevant parameters, it will further be possible to use 2-BIT data to convert the multiphoton action cross section into a multiphoton absorption cross section. 2-BIT therefore promises to be a powerful means of elucidating the photochemical and photophysical details of complex multiphoton processes through, for instance, comparison with nonlinear absorption data.

References

[1] Z. Tomova, N. Liaros, S. A. Gutierrez Razo, S. M. Wolf, and J. T. Fourkas, "In situ measurement of the effective nonlinear absorption order in multiphoton photoresists," *Laser Photonics Rev.*, vol. 10, no. 5, pp. 849–854, 2016.

[2] Boyd, "Boyd - Nonlin Optics," *J. Chem. Inf. Model.*, vol. 53, pp. 1689–1699, 2013.

[3] M. Göppert-Mayer, "Elementary processes with two quantum transitions," *Ann. der Phys.*, vol. 18, no. 7–8, pp. 466–479, 2009.

[4] J. H. Bechtel and W. L. Smith, "Two-photon absorption in semiconductors with picosecond laser pulses," *Phys. Rev. B*, vol. 13, no. 8, p. 3515, 1976.

[5] N. Liaros *et al.*, "NLO response of photoswitchable azobenzene-based materials," *ChemPhysChem*, vol. 14, no. 13, pp. 2961–2972, 2013.

[6] N. Liaros and J. T. Fourkas, "The Characterization of Absorptive Nonlinearities," *Laser Photonics Rev.*, vol. 11, no. 5, pp. 1–21, 2017.

[7] G. S. He, L. S. Tan, Q. Zheng, and P. N. Prasad, "Multiphoton absorbing materials: Molecular designs, characterizations, and applications," *Chem. Rev.*, vol. 108, no. 4, pp. 1245–1330, 2008.

[8] "F.r.m.s.," pp. 460–473, 1882.

[9] K. S. Lee, D. Y. Yang, S. H. Park, and R. H. Kim, "Recent developments in the use of two-photon polymerization in precise 2D and 3D microfabrications," *Polym. Adv. Technol.*, vol. 17, no. 2, pp. 72–82, 2006.

[10] J. Van Hoorick, H. Ottevaere, H. Thienpont, and P. Dubruel, *Polymer and Photonic Materials Towards Biomedical Breakthroughs*. 2018.

[11] H. B. Sun and S. Kawata, "Two-photon photopolymerization and 3D lithographic microfabrication," *Adv. Polym. Sci.*, vol. 170, pp. 169–273, 2004.

[12] V. N. Melissinaki, "Sensing Resonating Devices Fabricated on Optical Fibers Using Multi-photon Polymerization Technique," no. December, 2017.

[13] X. Zou and T. Izumitani, "Spectroscopic properties and mechanisms of excited state absorption and energy transfer upconversion for Er3+-doped glasses," *J. Non. Cryst. Solids*, vol. 162, no. 1–2, pp. 68–80, 1993.

[14] J. Glauber *et al.*, "Nonlinear Absorption of light: optical saturation of electronic transitions in organic molecules with high intensity laser radiation," *IEEE J. Quantum Electron.*, vol. 130, pp. 358–367,

1967.
[15] A. L. Smirl, K. M. Bohnert, K. Mansour, and S. C. Moss, “Simultaneous Measurement of the Two-Photon Coefficient and Free-Carrier Cross Section Above the Bandgap of Crystalline Silicon,” *IEEE J. Quantum Electron.*, vol. 22, no. 2, pp. 360–368, 1986.
[16] P. Tian and W. S. Warren, “Ultrafast measurement of two-photon absorption by loss modulation.,” *Opt. Lett.*, vol. 27, no. 18, pp. 1634–6, 2002.
[17] M. Sheik-Bahae, A. A. Said, T. H. Wei, D. J. Hagan, and E. W. Van Stryland, “Sensitive Measurement of Optical Nonlinearities Using a Single Beam,” *IEEE J. Quantum Electron.*, vol. 26, no. 4, pp. 760–769, 1990.
[18] I. Kang, T. Krauss, and F. Wise, “Sensitive measurement of nonlinear refraction and two-photon absorption by spectrally resolved two-beam coupling.,” *Opt. Lett.*, vol. 22, no. 14, pp. 1077–1079, 1997.
[19] N. Liaros, S. A. Gutierrez Razo, and J. T. Fourkas, “Probing Multiphoton Photophysics Using Two-Beam Action Spectroscopy,” *J. Phys. Chem. A*, vol. 122, no. 32, pp. 6643–6653, 2018.
[20] K. D. Nanda and A. I. Krylov, “Two-photon absorption cross sections within equation-of-motion coupled-cluster formalism using resolution-of-the-identity and Cholesky decomposition representations: Theory, implementation, and benchmarks,” *J. Chem. Phys.*, vol. 142, no. 6, pp. 1–13, 2015.
[21] J. P. Gordon, R. C. C. Leite, R. S. Moore, S. P. S. Porto, and J. R. Whinnery, “Long-transient effects in lasers with inserted liquid samples,” *J. Appl. Phys.*, vol. 36, no. 1, pp. 3–8, 1965.
[22] W. T. White, M. a. Henesian, and M. J. Weber, “Photothermal-lensing measurements of two-photon absorption and two-photon-induced color centers in borosilicate glasses at 532 nm,” *J. Opt. Soc. Am. B*, vol. 2, no. 9, p. 1402, 1985.
[23] J. R. Whinnery, “Laser Measurement of Optical Absorption in Liquids,” *Acc. Chem. Res.*, vol. 7, no. 7, pp. 225–231, 1974.
[24] J. Fischer, J. B. Mueller, A. S. Quick, J. Kaschke, C. Barner-Kowollik, and M. Wegener, “Exploring the mechanisms in sted-enhanced direct laser writing,” *Adv. Opt. Mater.*, vol. 3, no. 2, pp. 221–232, 2015.
[25] C. Decker and K. Moussa, “Real-Time Kinetic Study of Laser-Induced Polymerization,” vol. 4462, no. 24, pp. 4455–4462, 1989.
[26] J. Fischer, J. B. Mueller, J. Kaschke, T. J. A. Wolf, A.-N. Unterreiner, and M. Wegener, “Three-dimensional multi-photon direct laser writing with variable repetition rate,” *Opt. Express*, vol.

21, no. 22, p. 26244, 2013.
[27] L. Li and J. T. Fourkas, “Multiphoton polymerization,” *Mater. Today*, vol. 10, no. 6, pp. 30–37, 2007.
[28] Q. Hu, “Multiphoton Lithography Based 3D Micro/Nano Printing.”
[29] R. A. Farrer, F. L. Butterfield, V. W. Chen, and J. T. Fourkas, “Highly Efficient Multiphoton-Absorption-Induced Luminescence from Gold Nanoparticles,” *Nano Lett.*, vol. 5, no. 6, pp. 1139–1142, 2005.
[30] *Three-Dimensional Microfabrication Using Two-photon Polymerization*. 2016.
[31] M. Farsari, M. Vamvakaki, and B. N. Chichkov, “Multiphoton polymerization of hybrid materials,” *J. Opt.*, vol. 12, no. 12, 2010.